JULHO 2019

U.PORTO
FEUP FACULDADE DE ENGENHARIA
UNIVERSIDADE DO PORTO

# INTENSIFICATION OF OZONATION PROCESSES FOR WATER TREATMENT: OZONE/OXYGEN SEPARATION BY MEMBRANE

**CRISTIANA ANDREIA VIEIRA GOMES**
DISSERTAÇÃO DE MESTRADO APRESENTADA
À FACULDADE DE ENGENHARIA DA UNIVERSIDADE DO PORTO EM
ENGENHARIA QUÍMICA

Integrated Master in Chemical Engineering

# *Intensification of ozonation processes for water treatment: ozone/oxygen separation by membrane*

## Master's dissertation

by

**Cristiana Andreia Vieira Gomes**

**Developed for the dissertation course unit**

at

**Laboratório Associado LSRE-LCM**

**Laboratory of Separation and Reaction Engineering - Laboratory of Catalysis and Materials**

SRE CM
LABORATÓRIO ASSOCIADO
LABORATÓRIO DE PROCESSOS DE SEPARAÇÃO E REACÇÃO
LABORATÓRIO DE CATÁLISE E MATERIAIS

Supervisor: **Dr. Alexandre F. P. Ferreira**

Co-Supervisors: **Dr. Vítor Jorge Pais Vilar**

**Prof. Alírio Egídio Rodrigues**

U.PORTO
FEUP FACULDADE DE ENGENHARIA
UNIVERSIDADE DO PORTO

**Chemical Engineering Department**

**July of 2019**

**CLASSIFIED DOCUMENT. USE ONLY FOR EVALUATION PURPOSES**

“Some are born great,
some achieve greatness,
and some have greatness thrust upon them.”

William Shakespeare

# Agradecimentos

Deixo esta secção para agradecer às pessoas que contribuíram para a realização deste trabalho e que me acompanharam em todo este percurso académico.

Quero começar por agradecer aos meus orientadores, Doutor Alexandre Ferreira, Doutor Vítor Vilar e Professor Alírio Rodrigues, pela oportunidade e confiança depositada em mim para realizar este projeto. Um especial agradecimento ao orientador Doutor Alexandre Ferreira por me ter acompanhado e apoiado na realização deste projeto durante estes 5 meses.

Quero agradecer também à Ana Isabel Gomes pela ajuda na montagem da instalação experimental e na realização das experiências.

Agradeço aos meus pais por todo o apoio e força que me deram ao longo de toda a minha vida e pelo esforço feito para que eu pudesse chegar a este momento. Obrigada por nunca terem desistido de mim, mesmo nos momentos mais difíceis.

Às minhas amigas, Cláudia, Paixão, Bea, Carina, Maria João, Marques, Márcia e Daniela, pela companhia e amizade durante este percurso académico, por partilharem memes e por serem vocês próprias uns memes. Vocês tornaram-se a família que nunca pensei que seria possível ter.

À Marta Alves também o meu obrigado pela companhia no laboratório e pelos bons momentos de distração durante estes últimos 5 meses.

Por último, quero agradecer a todas as outras pessoas que também me ajudaram durante este percurso académico e que posso ter esquecido de referir aqui.

Este trabalho foi suportado por: Laboratório Associado LSRE-LCM - UID/EQU/50020/2019 - financiado por fundos nacionais através da FCT/MCTES (PIDDAC).

O Doutor Alexandre Ferreira, o Doutor Vítor Vilar e o Professor Alírio Rodrigues, orientadores desta dissertação, são membros integrados do Laboratório Associado LSRE-LCM - UID/EQU/50020/2019 - financiado por fundos nacionais através da FCT/MCTES (PIDDAC).

FCT
Fundação para a Ciência e a Tecnologia
MINISTÉRIO DA CIÊNCIA, TECNOLOGIA E ENSINO SUPERIOR

REPÚBLICA PORTUGUESA

# Abstract

Water pollution is an increasing problem in our days, not only because of the visible contamination but also the imperceptible one, such as toxins, pesticides, pharmaceutical compounds. One way to efficiently treat water and eliminate these components is ozonation - oxidation with ozone. However, this technique entails some problems, mainly in the ozone production through oxygen, since it requires high energetic costs (20 kWh/kg $O_3$ produced) and generates low quantities of $O_3$ (mass fraction of 10-15 %). So, this work's main objective was to evaluate the possibility of separating oxygen and ozone through a given membrane to increase the efficiency of ozonation.

First, mathematical models for the $O_3/O_2$ separation in two different membrane configurations, spiral wound (SWM) and hollow fiber (HF), and for the flow patterns that may appear in each one of the membranes (cross-flow in the SWM, and co-current, counter-current, and cross-flow in the HF membranes) were studied, allowing a better understanding of the different parameters influence in the efficiency of the separation.

The mathematical models for the hollow fiber membranes revealed that the counter-current flow is more efficient than the co-current and cross-flow patterns, as expected. The maximum differences observed between the three flow patterns were approximately 0.01-0.02 in the ozone permeate molar fraction and 0.1-0.2 $mol \cdot s^{-1}$ in the permeate outlet flow rate. As for the spiral wound membrane, the present study allowed a better understanding of the membrane operation, since the SWM only operates in cross-flow and a comparison between membranes with different geometries is not plausible.

The overall analysis showed that, regardless of the membrane geometry and the flow pattern, the effect of each parameter in the membrane performance is similar, *i.e.*, the permeate composition changes in the same direction. By increasing the membrane permeability of oxygen or ozone, the selectivity, the membrane dimensions or the feed pressure or decreasing the permeate pressure, it was verified that the permeate flow rate increases. As for the ozone permeate molar fraction, it decreases with the increase of the membrane permeability of $O_2$ or $O_3$ and the membrane dimensions, and increases with the variation of the other parameters.

The $O_3/O_2$ separation was also experimentally evaluated in a PDMS spiral wound membrane, in which the membrane permeances (ratio of the membrane permeability to the membrane thickness) of ozone and oxygen and the selectivity were estimated. The membrane permeance of pure oxygen was first determined, giving $8.45 \times 10^{-8}$ $mol \cdot m^{-2} \cdot s^{-1} \cdot Pa^{-1}$. In a mixture of $O_2$ and $O_3$, this ratio was equal to $7.47 \times 10^{-9}$ $mol \cdot m^{-2} \cdot s^{-1} \cdot Pa^{-1}$ for oxygen and $8.84 \times 10^{-9}$ $mol \cdot m^{-2} \cdot s^{-1} \cdot Pa^{-1}$ for ozone. The $O_3/O_2$ selectivity was found to be approximately equal to 1.3.

**Keywords:** ozone, oxygen, membrane, spiral wound module, hollow fiber module

# Resumo

A poluição da água é um problema cada vez maior nos nossos dias, não só devido à contaminação visível, mas também à impercetível, como as toxinas, pesticidas, compostos farmacêuticos. Uma forma eficiente de tratar a água e eliminar estes componentes é a ozonização – oxidação com ozono. No entanto, esta técnica envolve alguns problemas, principalmente na produção de ozono através de oxigénio, uma vez que requer altos custos energéticos (20 kWh/kg $O_3$ produzido) e produz baixas quantidades de $O_3$ (fração mássica de 10-15 %). Assim, o principal objetivo deste trabalho foi avaliar a possibilidade de separar oxigénio e ozono como uma dada membrana de forma a aumentar a eficiência da ozonização.

Primeiro, os modelos matemáticos para a separação de $O_3/O_2$ em duas membranas com configurações diferentes (espiral e fibras ocas) e para os tipos de escoamento que podem aparecer em cada uma delas (cross-flow nas membranas em espiral, e coocorrente, contracorrente e cross-flow nas membranas de fibras ocas) foram estudados, permitindo uma melhor compreensão do efeito de vários parâmetros na eficiência da separação.

Os modelos matemáticos para membranas com fibras ocas revelaram que o escoamento em contracorrente é mais eficiente do que coocorrente e cross-flow, como esperado. As diferenças máximas observadas nos três tipos de escoamento foram aproximadamente 0,01-0,02 na fração molar de ozono no permeado e 0,1-0,2 $mol \cdot s^{-1}$ no caudal de saída do permeado. Quanto às membranas em espiral, o presente estudo permitiu ter um melhor entendimento de como as membranas funcionam, já que estas apenas operam em cross-flow e uma comparação com membranas de diferentes geometrias não é muito plausível.

A análise geral mostrou que, independentemente da geometria da membrana e do tipo de escoamento, o efeito de cada parâmetro no desempenho da membrana é semelhante, ou seja, a composição do permeado varia no mesmo sentido. Aumentando a permeabilidade na membrana do oxigénio ou do ozono, a seletividade, as dimensões da membrana ou a pressão da alimentação ou diminuindo a pressão do permeado, verificou-se que o caudal de permeado aumentava. Quanto à fração molar de ozono no permeado, esta diminui com o aumento da permeabilidade na membrana do $O_2$ ou do $O_3$ e das dimensões da membrana, e aumenta com o aumento dos outros parâmetros.

A separação de $O_3/O_2$ também foi avaliada experimentalmente numa membrana em espiral de PDMS, na qual as permeâncias na membrana (razão da permeabilidade na membrana pela espessura da membrana) do ozono e do oxigénio e a seletividade foram estimadas. A permeância na membrana do oxigénio puro foi primeiro determinada, tendo dado $8{,}45\times10^{-8}$ $mol \cdot m^{-2} \cdot s^{-1} \cdot Pa^{-1}$. Numa mistura de $O_2$ e $O_3$, esta razão foi igual a $7{,}47\times10^{-9}$ $mol \cdot m^{-2} \cdot s^{-1} \cdot Pa^{-1}$ para

o oxigénio e $8{,}84\times10^{-9}$ $mol\cdot m^{-2}\cdot s^{-1}\cdot Pa^{-1}$ para o ozono. A seletividade de $O_3/O_2$ foi aproximadamente igual a 1,3.

**Palavras-chave:** ozono, oxigénio, membrana, módulo de espiral, módulo de fibras oca

# Declaration

I hereby declare, on my word of honor, that this work is original and that all non-original contributions were properly referenced with source identification.

Porto, 1 of July of 2019

*(Cristiana Andreia Vieira Gomes)*

# Index

# List of Figures

# List of Tables

# Notation and Glossary

| | | |
|---|---|---|
| $A$ | Total exchange area | $m^2$ |
| $B$ | Permeability of the spacing material inside a spiral wound membrane | $m^2$ |
| $C_{g,i}$ | Concentration in the bulk of species $i$ | $mol \cdot m^{-3}$ |
| $C_{g,m,i}$ | Concentration at the membrane surface of species $i$ | $mol \cdot m^{-3}$ |
| $d$ | Membrane thickness | m |
| $d_e$ | External diameter of each fiber in a hollow fiber module | m |
| $d_i$ | Internal diameter of each fiber in a hollow fiber module | m |
| $D_i$ | Diffusivity of species $i$ | $m^2 \cdot s^{-1}$ |
| $D_{ln}$ | Logarithmic mean diameter of each fiber in a hollow fiber module | m |
| $F_p$ | Generic permeate side flow rate | $mol \cdot s^{-1}$ |
| $J_i$ | Membrane flux of species $i$ | $mol \cdot m^{-2} \cdot s^{-1}$ |
| $k_{g,i}$ | Film side mass transfer coefficient for species $i$ | $m \cdot s^{-1}$ |
| $l$ | Hollow fiber length variable or spiral wound length space dimension | m |
| $L$ | Membrane length of a hollow fiber or a spiral wound | m |
| $L_{p,i}$ | Membrane permeability of species $i$ | $mol \cdot m \cdot m^{-2} \cdot s^{-1} \cdot Pa^{-1}$ |
| $n$ | Molar quantity of a given gas | mol |
| $N_f$ | Number of fibers in a hollow fiber module | |
| $P$ | Pressure | Pa |
| $P_f$ | Feed pressure | Pa |
| $P_p$ | Permeate side pressure | Pa |
| $P_{p,0}$ | Permeate outlet pressure | Pa |
| $Q_f$ | Volumetric feed flow rate | $m^3 \cdot s^{-1}$ |
| $Q_r$ | Volumetric retentate flow rate | $m^3 \cdot s^{-1}$ |
| $R$ | Ideal gas constant | $Pa \cdot m^3 \cdot mol^{-1} \cdot K^{-1}$ |
| $S_i$ | Membrane solubility of species $i$ | $mol \cdot m^{-3} \cdot Pa^{-1}$ |
| $t$ | Time | s |
| $t_f$ | Feed/retentate spacer thickness in a spiral wound membrane | m |
| $t_p$ | Permeate spacer thickness in a spiral wound membrane | m |
| $T$ | Temperature | K |
| $u$ | Feed/retentate side flow rate per unit length | $mol \cdot m^{-1} \cdot s^{-1}$ |
| $u_f$ | Feed flow rate per unit length | $mol \cdot s^{-1}$ |
| $u_r$ | Retentate flow rate per unit length | $mol \cdot s^{-1}$ |
| $U$ | Feed/retentate side flow rate | $mol \cdot s^{-1}$ |
| $U_1$ | Feed/retentate side flow rate of the more permeable component (species 1) | $mol \cdot s^{-1}$ |
| $U_2$ | Feed/retentate side flow rate of the less permeable component (species 2) | $mol \cdot s^{-1}$ |
| $U_f$ | Feed flow rate | $mol \cdot s^{-1}$ |
| $U_r$ | Retentate flow rate | $mol \cdot s^{-1}$ |
| $v$ | volume | $m^3$ |
| $V$ | Permeate side flow rate | $mol \cdot s^{-1}$ |

| | | |
|---|---|---|
| $V_0$ | Permeate flow rate at the outlet | mol·s$^{-1}$ |
| $V_1$ | Permeate side flow rate of the more permeable component (species 1) | mol·s$^{-1}$ |
| $V_2$ | Permeate side flow rate of the less permeable component (species 2) | mol·s$^{-1}$ |
| $w$ | Spiral wound module width space dimension | m |
| $W$ | Membrane leaf width of a spiral wound membrane | m |
| $x$ | Feed/retentate side molar fraction of the more permeable component | |
| $x_{\mathrm{f}}$ | Feed molar fraction of the more permeable component | |
| $x_{\mathrm{f},i}$ | Generic feed molar fraction of species $i$ | |
| $x_{\mathrm{r}}$ | Retentate molar fraction of the more permeable component | |
| $y$ | Permeate side molar fraction of the more permeable component in the bulk stream | |
| $y'$ | Permeate molar fraction of the more permeable component on the membrane surface | |
| $y_0$ | Average molar fraction of the more permeable component at the permeate outlet | |
| $y_{\mathrm{f}}^{'}$ | Permeate molar fraction of the more permeable component on the membrane surface at the feed inlet | |
| $y_{\mathrm{p},i}$ | Generic permeate molar fraction of species $i$ | |
| $y_{\mathrm{r}}^{'}$ | Permeate molar fraction of the more permeable component on the membrane surface at the retentate outlet | |
| $y_{\mathrm{r},i}$ | Generic retentate molar fraction of species $i$ | |
| $z$ | Membrane thickness variable | m |

*Greek Letters*

| | | |
|---|---|---|
| $\alpha$ | Membrane selectivity (permeability of more permeable component/permeability of less permeable component) | |
| $\alpha_{ij}$ | Generic membrane selectivity (permeability of species $i$/ permeability of species $j$) | |
| $\gamma$ | Ratio of permeate pressure to feed pressure | |
| $\mu$ | Viscosity of the permeate gas mixture | Pa·s |

***List of Acronyms***

| | |
|---|---|
| ABS | Acrylonitrile Butadiene Styrene |
| AC | Activated Carbon |
| ID | Interior Diameter |
| HF | Hollow fiber |
| MMM | Mixed Matrix Membrane |
| OD | Outside Diameter |
| ODE | Ordinary Differential Equation |
| PDD | Perfluoro-2,2-Dimethyl-1,1,3-Dioxole |
| PDMS | Polydimethyl Siloxane |
| PES | Polyethersulfone |

| | |
|---|---|
| PP | Polypropylene |
| PSA | Pressure Swing Adsorption |
| PTFE | Polytetrafluoroethylene |
| PVAc | Poly(vinyl acetate) |
| PVDF | Polyvinylidene Difluoride |
| SWM | Spiral Wound Membrane |
| TFE | Tetrafluoroethylene |
| UV | Ultraviolet |
| VOC | Volatile Organic Compound |

# 1 Introduction

## 1.1 Framing and presentation of the work

Due to the increase of water pollution by chemical compounds of difficult elimination, such as pesticides and pharmaceutical compounds [1, 2], it is more and more critical the application of techniques that remove these pollutants with high efficiency.

There are several methods to treat the water with this intend, such as ozonation, adsorption and ultraviolet radiation [3]. In this work, ozonation was the method given more emphasis, since it is being increasingly used in this area and, by being a strong oxidant, ozone can oxidize a wide variety of organic and inorganic matter [4, 5]. However, ozone production through oxygen requires high energetic costs (20 kWh/kg $O_3$ produced) and generates low quantities of $O_3$ (mass fraction of 10-15 %). These limitations difficult the solubility of the gas in the water and reduces the efficiency of the process [6].

The possible approaches to minimize these limitations are the use of pressurized ozone reactors (2-7 atm) or the separation of oxygen and ozone [7, 8]. The objective of this work is to explore the separation of $O_3/O_2$, obtaining an ozone-enriched stream, and recirculating the non-converted oxygen back to the ozone generator.

There are several technologies to separate $O_3/O_2$ (*e.g.*, adsorption, ozone condensation, ozone dissolution in solvents), but the most promising one is membrane separation, since it is a process with short contact time, not allowing a significant ozone decomposition, and it does not involve hazardous compounds [9, 10].

To achieve the objective of this work, mathematical models for the $O_3/O_2$ separation in two different membrane configurations (hollow fiber and spiral wound) were studied and simulated. It was also evaluated a PDMS spiral wound membrane experimentally.

## 1.2 Outline

The present work is divided into six main chapters: introduction, context and state of the art, materials and methods, results and discussion, conclusions, and assessment of the work done.

In Chapter 1, the motivation for the study of ozone/oxygen separation and its framing in a concrete application is briefly described. To achieve such separation, the ozone properties, applications, different separation processes, and their limitations are introduced in Chapter 2.

Chapter 3, materials and methods, describes the mathematical models used to analyze the flow in the two membrane configurations in study, the experimental setup and experimental procedures to study the ozone/oxygen separation in a spiral wound membrane.

Chapter 4 contains the analysis realized with the mathematical models and the experimental results.

In Chapter 5, the main conclusions of this work are summarized.

Chapter 6 presents the information about the achieved objectives, the limitations, and future work.

## 1.3 Contributions of the Work

The work I have done for this dissertation started in the previous semester, with a research for different studies with ozone and oxygen, in which they had used adsorption or membranes. This would help to make a first evaluation of if it would be possible to separate $O_3$ and $O_2$ with one of those methods and what types of material and equipment would be necessary.

As for the semester in which the dissertation was developed, I continue the research for more literature in the subject. Then I simulated the mathematical models found for different membrane configurations (spiral wound and hollow fiber modules) in Scilab 6.0.1, writing the codes necessary for that. In the experimental part of this work, I search for suppliers to acquire a PDMS membrane and other equipment, like compressors. I also made all the experimental tests presented in this work.

# 2 Context and State of the Art

## 2.1 Ozone Properties

Ozone is a very unstable molecule with a short half-life which promotes its inclination to fall back into its original state, *i.e.*, in the form of oxygen molecules ($O_2$). This fact makes $O_3$ a strong oxidant, that can be used to destroy organic and inorganic matter and microorganisms. This phenomenon is designed as ozonation [4, 11].

Due to its instability, it is essential to have into account the physical and chemical properties of ozone, such as boiling temperature, density, solubility in water, half-life, before its usage. The more relevant physical and chemical properties are summarized in Table 1.

Two of the most crucial ozone properties are its solubility in water and half-live in water and on air, since their values depend on various factors and affect the efficiency of ozone utilization. Half-live is related to the time that takes to half of the ozone quantity, in a gaseous or liquid solution, to disappear, due to its decomposition in oxygen. Factors influencing this value are temperature, pH, environment, UV light, the concentration of ozone, and solution purity [12]. Regarding its solubility in water, this one varies with temperature, pressure, and ozone concentration on the gaseous stream. This dependency can be observed in Figure 1 [13].

*Table 1 – Physical and chemical properties of ozone [4, 11, 12, 14]*

| | |
|---|---|
| **Molecular weight / g·mol$^{-1}$** | 48.00 |
| **Boiling temperature / °C** | -112 |
| **Density at 0 °C and 1 bar / kg·m$^{-3}$** | 2.142 |
| **Electrical potential / V** | 2.07 |
| **Standard heat of formation / kJ·mol$^{-1}$** | 142.12 |
| **Half-live in the water at 20 °C (pH 7) / min** | 20 |
| **Half-live on air at 20 °C / days** | 3 |

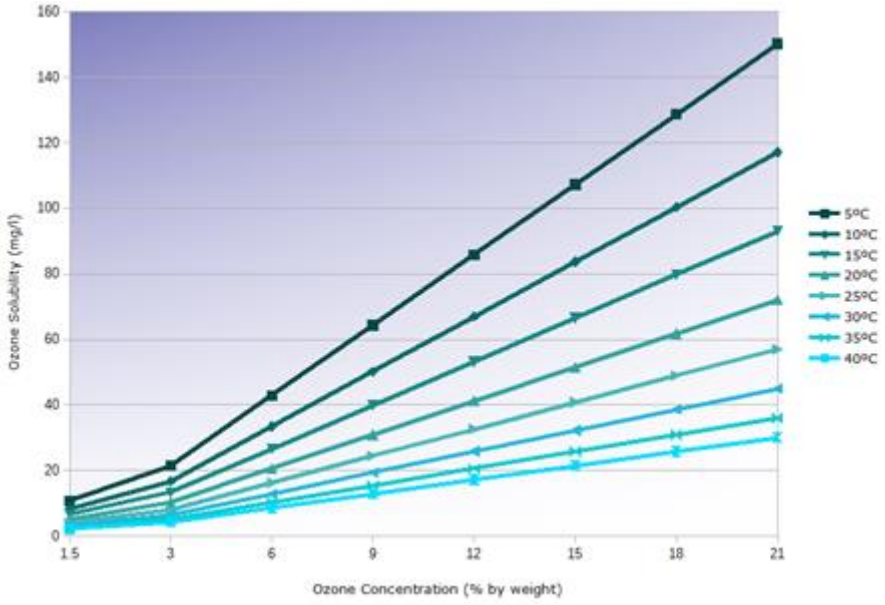


*Figure 1 - Solubility of ozone in water at 1 bar (adapted from [13])*

Long term exposure to ozone may cause symptoms like throat and mouth dryness, coughing, headaches, and irritation of eyes and respiratory system. To prevent these health risks, it was established maximum concentrations of ozone that a human being could be exposed to during a given period of time. For example, for exposure of eight hours per day, five days a week, the maximum admitted concentration is of 0.06 ppm. Since ozone has a distinctive odor, it is easy to detect it [4, 6, 15].

## 2.2 Ozone Applications

As a result of the above-mentioned properties and characteristics of ozone, this compound has different applications, for example, purification of water and air, food processing, medical treatments, elimination of odor from fire, animals or industrial processes [6, 16]. All these applications follow the same principle of ozone usage – ozonation.

In an aqueous surrounding, oxidation may happen by direct (with $O_3$) and indirect reaction mechanisms. The last one occurs due to the formation of reactive oxygen species, mainly $^{\bullet}OH$ radicals. Hydroxyl radicals are oxidants stronger than $O_3$, present a redox potential of 2.86 and have a much smaller half-life, $\sim 10^{-9}$ seconds. One kind of reaction will dominate, depending on the temperature, pH, and chemical composition of the aqueous solution [6, 14].

The application that will be the focus of this project is water treatment since it is the area with more use of ozone [5].

### 2.2.1 Drinking Water Treatment

In the drinking water treatment, ozone is used to decompose all kinds of organic matter, from algae and bacteria to pesticides and pharmaceutical compounds. However, depending on the type of compounds to be eliminated by ozonation, this method is applied in different steps of the drinking water treatment, promoting a pre-oxidation, intermediate/main oxidation or disinfection [1, 17].

In pre-oxidation, ozone is used to break down the structure of colloidal particles and macromolecules, enhancing coagulation and flocculation performance, reducing turbidity, taste and odor [2, 17].

In intermediate/main oxidation the purpose of ozone is to oxidize a more extensive variety of organic matter, *e.g.*, algae, pesticides, detergents, toxins, pharmaceutical compounds. The efficiency of ozonation varies according to the chemical structure of the undesired compounds and the environmental conditions. If the efficiency is not the desired, it can be used a combination of ozone with hydrogen peroxide [2, 17].

This type of advanced oxidation is subject to authorization because some by-products formed can fall within the scope of regulations (case of oxidation of bromides, chlorates, and iodates). In particular, the oxidation of bromides produces bromates, which are potentially carcinogenic [2, 6].

In disinfection, the objective of ozonation is to destroy pathologic microorganisms, making water drinkable [1].

The ozonation reactors are chambers made up of several compartments, in which the water passes through. The number of compartments depends on the kind of oxidation executed [2, 14]. Regarding the gaseous stream that transports the ozone, it is introduced in the reactor through gas-liquid contactors, such as bubble diffusers, injectors, and static mixers [18].

Due to its fast decomposition, ozone is produced *in situ* through a generator, using UV light or Corona process (electrical discharge). Both methods promote the rupture of oxygen molecules in radicals, that bond to other $O_2$ molecule, creating ozone [14, 19].

### 2.2.2 Limitations

One major obstacle to wider use of ozone is its high associated $O_3$ generation costs (20 kWh/kg $O_3$ produced), resulting from the fact that only a small fraction of the initial oxygen stream is converted into ozone ($O_3$ mass fraction of 10-15 %) [6, 10]. One novel approach to reduce such requirements is to separate ozone from oxygen, producing an ozone-enriched gas stream in which non-converted oxygen can be recirculated back to the ozonizer.

Another major limitation of current ozonation technologies is the high ozone supply demands, the long contacting time required in the reactor, and the bulky size of the equipment. These disadvantages are associated with the low ozone mass transfer rates from gas to liquid phase (solubility ratio from 30-40 %) [6]. Increasing the solubility of ozone in water and enhancing its degree of mixing can improve mass transfer. According to Henry's law, two options are available to increase ozone content in the water at a constant temperature: 1) increasing the pressure of the dissolution system or 2) reducing the amount of oxygen that is to be dissolved. As a result, the use of ozone-enriched streams and pressurized ozone reactors (2-7 atm) have been the subject of recent studies [7, 8].

## 2.3 Ozone/Oxygen Separation

There are different ways to separate $O_3$ and $O_2$, for instance, ozone condensation, ozone dissolution in solvents, adsorption, and membranes. The two first methods required harmful compounds and/or suitable precautions [9, 10]. For that motive, we are going to focus only on separation through adsorption and membranes.

With adsorption, it is possible to separate ozone and oxygen by passing the gaseous stream through various adsorption columns in series or a P(T)SA (pressure (temperature) swing adsorption). Independent of the apparatus adopted, silica gel and high silica zeolites are the adsorbents more used, once they are the most efficient for the desired separation and do not promote the ozone decomposition [9, 10, 20]. One of the studies that investigated the ozone/oxygen separation through adsorption used a PSA with a high silica zeolite (silicalite-1) and managed to enrich an oxygen-ozone stream from 5 % to 20 % in ozone mass fraction [20].

Typically, $O_3$ is the compound adsorbed and is carried into the ozone application by means of an inert gas stream, like nitrogen. The unadsorbed oxygen is recycled back to the ozone generator. However, since $O_3$ can only be desorbed on the purge phase and has a short half-life, it is difficult to recover the ozone product stream from the adsorption equipment without some decomposition [21, 22]. So, it is essential to have into account the half-life and the time that each adsorption/desorption cycle takes, before implanting this method.

This technology can be implemented with the operating conditions presented in Table 2. According to these values, the amount of ozone that can be adsorbed is as higher as the lower the temperature is or as higher the applied pressure is [23].

*Table 2 – Operation conditions for P(T)SA processes [23, 24]*

| | *Adsorption* | *Desorption* |
|---|---|---|
| **Temperature / ºC** | -100 to -30 | 0 to 50 |
| **Pressure / bar** | 1.1 to 5 | 0.5 to 1.5 |

Regarding the use of membranes in ozonation, several studies analyzed different aspects, such as mass transfer rates from gas to liquid phase and separation of oxygen and ozone, using polymeric and ceramics membranes [25].

Ceramic membranes are most used as gas-liquid contactors to study the ozone mass transfer to the liquid phase and improve $O_3$ solubility in water. This is an alternative to conventional contactors, since it creates a fixed barrier, without mechanical agitation, and improves problems like volume flow, viscosity and density fluctuation of both gas and liquid [26, 27]. Although these studies mention the possibility of separating $O_3/O_2$ with the apparatus used, they do not analyze the quality of the separation.

Even though polymeric membranes are often excluded from experiments with ozone, due to its high reactivity and easy degradation of these materials, studies show that PTFE, PVDF, PDMS and PP membranes have a specific resistance to $O_3$, making it possible to use on ozone/oxygen separation [28].

Besides polymeric membranes resistance to ozone, properties like membrane permeability, selectivity, diffusivity, and mass transfer coefficients are also a target of study for $O_3/O_2$ separation. Shanbhag and Sirkar (1998) described the membrane permeability and selectivity of oxygen, nitrogen, and ozone in three non-porous PDMS capillary membranes (SILCAP #1, SILCAP #5 and NEWCON #1), with different dimensions and number of capillaries, at room temperature and atmospheric pressure. Each membrane had a treatment prior to the measurements. SILCAP #5 was a freshly prepared module, not exposed to anything. SILCAP #1 had been exposed to ozone for a period of about 50 hours. While NEWCON #1 had been exposed to both ozone and fluorocarbon phase for a period of 80 hours, as part of a study to remove VOCs from air from the same authors. The dimensions and results obtained for each membrane are briefed in Table 3, and it was concluded that the membrane permeability of $O_3$ in PDMS is four times greater than that of $O_2$ on the three membranes, regardless of the pre-treatment made [29, 30]. Pines et al. (2005) explored the mass transfer rate of $O_3$ through porous PTFE and PVDF membranes and non-porous PTFE membranes using sheet contactor systems, at room temperature and transmembrane pressure between 0.0135 and 0.069 bar, to avoid bubble formation. They reported that most of the obtained data were in good agreement with the mass transfer correlations found in the literature [29, 31].

*Table 3 – Dimensions and results of each PDMS membrane [29, 30]*

| | *SILCAP #1* | *SILCAP #5* | *NEWCON #1* |
|---|---|---|---|
| **Capillaries ID/OD/ cm** | 0.16/0.24 | 0.03/0.06 | 0.03/0.06 |
| **Module length / m** | 0.28 | 0.22 | 0.38 |
| **Number of capillaries** | 4 | 98 | 25 |
| **Membrane permeability of $O_3$ / mol·m$^{-1}$·s$^{-1}$·Pa$^{-1}$** | $1.05\times10^{-12}$ | $8.83\times10^{-13}$ | $8.18\times10^{-13}$ |
| **Membrane permeability of $O_2$ / mol·m$^{-1}$·s$^{-1}$·Pa$^{-1}$** | $2.81\times10^{-13}$ | $2.24\times10^{-13}$ | $2.03\times10^{-13}$ |

The installation used to separate oxygen and ozone with membranes must involve an ozone generator, a membrane separation unit, gas pumping equipment (blowers, compressors…), and valves. Regarding the operating conditions, they are summarized in Table 4 [22, 32].

*Table 4 – Operating conditions for membrane separation processes [22, 32]*

| | | *Preference* |
|---|---|---|
| **Temperature / ºC** | -80 to 200 | 0 to 30 |
| **Pressure / bar** | 1 to 15 | 2 to 10 |

In all the referred membrane studies and patents, the ozone-enriched stream is the permeate, allowing the prospect to use the membranes as gas-liquid contactors, and the oxygen-enriched stream is the retentate that is recycled back to the $O_3$ generator [22, 32].

The most suitable membranes to use as contactors are those that are hydrophobic and organophobic, *i.e.*, those that have a low permeability to water and organic compounds, such as PDMS membranes and PDD-TFE copolymer [22, 32].

To maintain a high ozone driving force in the membrane, ozone must be continuously removed from the permeate zone. This can be accomplished by evacuating this zone with a suitable vacuum-producing means (vacuum pumps, venturi devices), positioned after the membrane separation unit, or with a carrier gas, that does not react with ozone, has a low membrane permeability and which is not incompatible with the intended purpose of ozone. Useful carrier gases include helium, nitrogen, argon, and carbon dioxide [22, 32].

One other way to separate the target mixture is by using mixed matrix membranes (MMM), that consists of incorporation of inorganic materials in the polymer matrix. MMMs exhibit several process benefits, such as time efficiency, energy saving, low membrane fouling, and flexible and straightforward large-scale operation [33, 34].

The potential of MMMs has been examined for several combinations of inorganic compounds and polymers, such as PVAc/4A zeolites, ABS/AC, PES/5A zeolites, in different gas separations, including air separation (e.g. $O_2/N_2$), natural gas separation (e.g. $CO_2/CH_4$), and hydrogen recovery (e.g. $H_2/CO_2$, $H_2/N_2$ and $H_2/CH_4$). Such studies reported an improvement in separation efficiency [33].

For the $O_3/O_2$ separation, the MMM more relevant is PDMS/silicalite-1, since there are studies, mentioned previously, reporting the separation of these gases with these materials alone.

Several investigators explored the membrane permeability of some gases, $O_2$, $N_2$, $CO_2$, $CH_4$, with PDMS membranes filled with silicalite-1. They stated that the addition of this adsorbent enhanced the membrane permeability of gases, exceeding those pertaining to the neat PDMS membrane, not changing the standard order of the gas membrane permeability ($CO_2$ > $CH_4$ > $O_2$ > $N_2$) [35, 36].

With all the information presented, it can be expected that the membrane permeability of ozone is also going to increase with a PDMS/silicalite-1 mixed matrix membrane.

### 2.3.1 Membrane Separation

A generic membrane separation, illustrated in Figure 2, takes place when a driving force acts on a particular component, to be preferably removed, allowing its transport through the membrane. This driving force consists in a chemical potential difference or electrical potential difference, *e.g.*, a pressure or concentration difference, across the membrane thickness, $d$, has a proportional relationship with the flux across the membrane, $J_i$ [37].

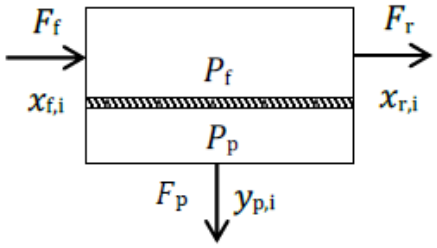


*Figure 2 - Scheme of a generic membrane separation [37]*

The description of the flux of a given fluid through a membrane is based in the Fick's first law and is given by:

$$J_i = \frac{F_p\, y_{p,i}}{A} = \frac{L_{p,i}}{d}\,(P_f x_{f,i} - P_p y_{p,i}) \quad (1)$$

The membrane permeability coefficient of species $i$, $L_{\mathrm{p},i}$, can be expressed in S.I. units ($mol \cdot m \cdot m^{-2} \cdot s^{-1} \cdot Pa^{-1}$) or in Barrer units (1 Barrer = $10^{-10}$ $cm^3(STP) \cdot cm \cdot cm^{-2} \cdot s^{-1} \cdot cmHg^{-1}$). Membrane permeability is an essential parameter in the characterization of membrane separation, as the selectivity ($\alpha_{ij}$).

There are two types of selectivity, the ideal one and the real one. The ideal selectivity is determined by the ratio between the membrane permeabilities of species $i$ and $j$. As for the real selectivity is determined with the species $i$ and $j$ molar fractions, according to Equation 2. These two parameters ($L_{\mathrm{p},i}$ and $\alpha_{ij}$) determine the capability of permeation in a membrane of a certain species and the potential of the membrane to separate species $i$ and $j$, respectively [37].

$$\alpha_{ij} = \frac{y_{\mathrm{p},i}}{y_{\mathrm{p},j}} \frac{y_{\mathrm{r},j}}{y_{\mathrm{r},i}} \tag{2}$$

*Flow patterns*

The fluid flow in a membrane can be described by one of the following ideal patterns: 1) co-current, in which both feed and permeate streams are in plug flow and go in the same direction; 2) counter-current, in which both feed and permeate streams are also in plug flow, but go in opposite directions; and 3) cross-flow, in which the feed stream is in plug flow and flows parallel to the membrane, whereas the permeate stream flows perpendicular to it and the portion of gas that was permeated, in a given point, does not mix immediately with the main product stream. So, there is a difference between the local concentration (on the membrane surface) and the concentration in the bulk stream. Generally, counter-current gives the best performance followed by cross-flow and co-current [38, 39]. A schematic of each pattern is presented in Figure 3.

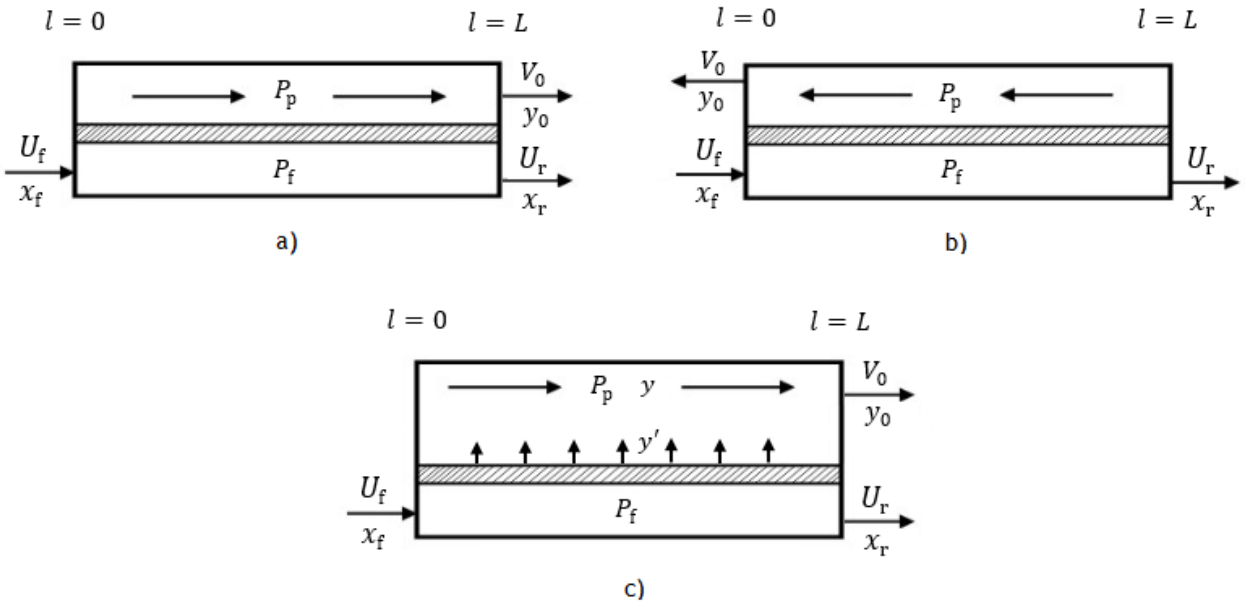


*Figure 3 - Schematics of a co-current, a), counter-current, b), and cross-flow, c), patterns [38]*

*Module configuration*

The types of membrane modules used currently have the form of a plate-and-frame, spiral wound, tubular or hollow fiber. Figure 4 shows a scheme of each module configuration. In the plate-and-frame module, the membrane, feed and product spacers are layered together, like in a sandwich between two end plates, and is mainly operated in cross-flow. This type of configuration presents the most straightforward design, but it has the lowest efficiency and a high-pressure drop. The spiral wound configuration consists of a plate-and-frame system wrapped around a central perforated pipe, that collects the permeate, and almost always operates in the cross-flow pattern. This module configuration is easy to clean and offers a larger mass transfer area than plate-and-frame membranes. It is used in a wide variety of applications since it can have multiple arrangements with different spacers, membrane types, lengths, widths, and diameters. The hollow fiber and tubular modules are constituted of fine capillaries or tubes, respectively, housed like a shell and tube heat exchanger, and can operate in any flow pattern. Tubular modules have high operating costs but have less fouling than plate-and-frame and similar fouling as a spiral wound module. The hollow fiber configuration has a larger exchange area than tubular modules, however, has irreversible fouling and fiber breakage [40-42].

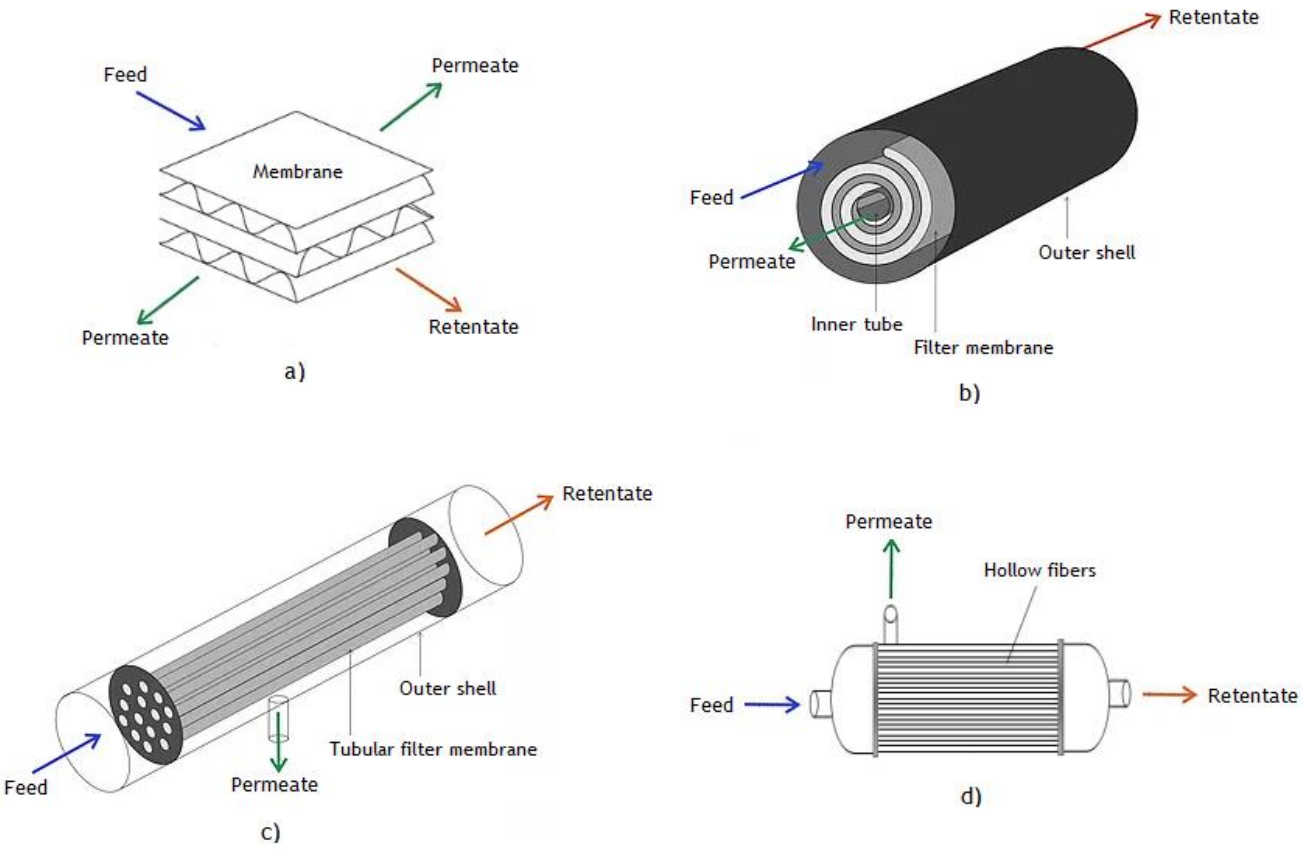


*Figure 4 – Schematics of a plate-and-frame, a), a spiral wound, b), a tubular, c), and a hollow fiber, d), module configurations [40, 43]*

*Transport mechanisms*

According to the porosity of the membrane matrix, different transport mechanisms may appear in a membrane, including Poiseuille (viscous) flow, Knudsen's diffusion, molecular sieving, capillary condensation, and solution–diffusion mechanism.

In Knudsen's diffusion, the particles interact with the pore walls much more frequently than colliding with one another, which allows lighter molecules to diffuse through the pores preferentially. Contrarily, Poiseuille or viscous flow predominates when there are more collisions between the particles than with the pores walls.

To function as a molecular sieve, membranes must have pore diameters similar to the size of the particles to be separated. In this case, the smaller molecules are permeated.

Gas separation can also be affected by partial condensation of some of the components in the pores, with the consequential transport of the condensed molecules across the pores.

Transport of molecules by solution-diffusion mechanism consists of three steps: 1) sorption of the preferential compound at the feed side of the membrane; 2) activated diffusion through the membrane; and 3) desorption in the permeate zone [37, 44].

The first four mechanisms mentioned are more relevant in porous membranes, that are mostly applied in microfiltration and ultrafiltration. However, in a liquid separation, the Knudsen's diffusion is generally not observed, since the molecules are closer to each other, predominating the collisions between particles. In practical situations, there will be a distribution of pore sizes in the membrane; thus the separation is influenced by a combination of these transport mechanisms, *i.e.*, the separation is largely affected by the pores size distribution. The membrane permeability coefficient can be calculated from known data *a priori* of practical tests. However, this type of membrane was left out of the context of this work, since it is not of interest for the case in study [37].

Solution-diffusion is the main transport mechanism on non-porous membranes, which are used for gas separation and pervaporation. In this type of membranes, the separation occurs at a molecular level, where the membrane solubility, $S_i$, and membrane diffusion, $D_i$, coefficients characterize the gas separation, according to Equation 3 [37]. For dense membranes, several models to determined membrane permeability were developed, such as molecular, free volume, Flory-Huggins, dual-mode sorption, partial immobilization models [45]. Nevertheless, these models were left out of the context of this work, giving that they required specific parameters that differ from component to component.

$$L_{\mathrm{p},i} = S_i \times D_i \tag{3}$$

Besides the diffusion through the membrane, it can also exist a gas concentration variation in the film layer, between the fluid and the membrane, according to the film theory. In this region, the flux is described by the following expression:

$$J_i = k_{\mathrm{g},i} \left(C_{\mathrm{g},i} - C_{\mathrm{g,m},i}\right) \tag{4}$$

The film theory can be considered on both sides of the membrane, *i.e.*, in the feed/retentate side and the permeate side of the membrane [46].

Combining all the mass transfer mechanisms in gas separation, it is obtained an overall mass transfer coefficient that describes all the mass resistance terms.

In the case of the flux varies with position and time, *i.e.*, a transient state, it is used Fick's second law (Equation 5) [37].

$$\frac{\partial C_{\mathrm{g},i}}{\partial t} = -\frac{\partial J_i}{\partial \mathrm{z}} = D_i \frac{\partial^2 C_{\mathrm{g},i}}{\partial z^2} \tag{5}$$

# 3 Materials and Methods

This work was divided into two parts: 1) modeling, in which the mathematical model for two different membrane geometries (spiral wound and hollow fiber) were studied; and 2) experimental evaluation of the $O_3/O_2$ separation in a selected membrane.

## 3.1 Mathematical Models

### 3.1.1 Spiral Wound Membrane

Before explaining the mathematical model for a spiral wound membrane (SWM), it is useful first to understand how this membrane is assembled and works. As shown in Figure 5, spacing material is placed between two flat membrane sheets, to allow the passage of the permeate and feed/retentate streams. This constitutes one membrane leaf, and the module may have several leaves. In the permeate side, three edges of the membrane sheets are glued together, and the open border is sealed to a perforated central tube. This forces the permeate to flow mainly perpendicularly to the central tube and ensures that the two streams (feed/retentate and permeate) do not mix with each other. The feed/retentate stream flows predominantly parallel to the central tube. The assembly is rolled around the central tube, that collects the permeate stream, and placed inside a pressure vessel [47, 48].

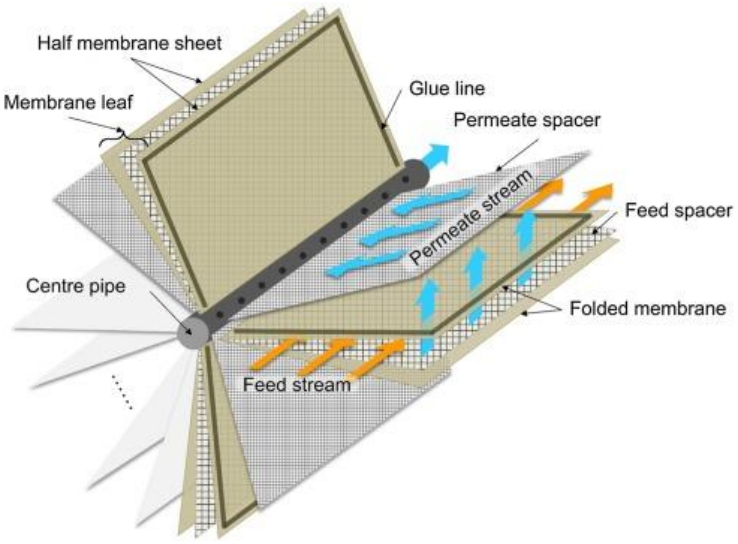


*Figure 5 - Schematics of a spiral wound membrane internal structure [48]*

Different mathematical models and studies with spiral wound membranes are available in the literature. One reason for this is that accurate modeling needs to have into account the two-dimensional nature of the fluid flow. Some of the available models for SWM were developed by Pan (1983), Qi and Henson (1997), and Krovvidi et al. (1992). The last two are based on the

model earlier developed by Pan with some approximations and simplifications, so the model selected to analyze the system in this study was the full model developed by Pan [41].

The mathematical formulation for the permeation of the SWM is based on the schematics presented in Figure 6 and on the following assumptions [41, 49]:

1. The feed stream flows through the skin side of the membrane.
2. No mixing of permeate fluxes of different compositions occurs inside the porous supporting layers of the membrane (spacing layers).
3. Feed flow in the spiral direction and permeate flow in the axial direction is neglected.
4. The resistance to gas flow in the feed/retentate and permeate spacers is consider insignificant.
5. Membrane permeability is constant, independent of pressure and temperature.
6. Feed/retentate gas pressure drop is negligible.
7. Permeate pressure varies only in the permeate flow direction and is described by Darcy law.
8. Channel curvature is neglected, and the membrane is treated as a flat sheet with a cross-flow pattern.
9. The gas mixture is treated as ideal.
10. Steady state is assumed.
11. All membranes in the module are identical.

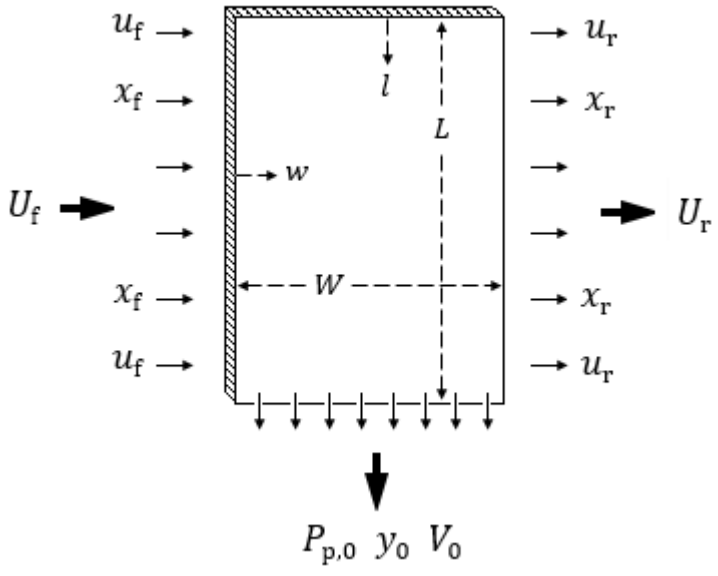


*Figure 6 - Scheme of one leaf unrolled of a spiral wound module [49]*

Under the previous assumptions and according to the schematics of Figure 6, the transport equations for a binary mixture in a spiral wound permeator are the following:

Permeation:

$$\left[\frac{\partial(ux)}{\partial w}\right]_l = -2\left(\frac{L_{p,1}}{d}\right)\left(P_f x - P_p y'\right) \quad (6)$$

$$\left[\frac{\partial[u(1-x)]}{\partial w}\right]_l = -2\left(\frac{L_{p,2}}{d}\right)\left[P_f(1-x) - P_p(1-y')\right] \quad (7)$$

$$\frac{d(ux)}{du} = y' \quad (8)$$

$$\frac{d[u(1-x)]}{du} = 1 - y' \quad (9)$$

Permeate pressure drop:

$$\frac{d\left(P_p{}^2\right)}{dl} = -\frac{RT\mu V}{W t_p B} \quad (10)$$

Material balance:

$$\frac{dV}{dl} = u_f - u_r \quad (11)$$

$$\frac{d(Vy)}{dl} = u_f x_f - u_r x_r \quad (12)$$

The factor of 2 in Equations 6 and 7 is due to each membrane leaf contains two membrane sheets. The retentate flow and molar fraction, $u_r$ and $x_r$, in Equations 11 and 12, are not constant and vary with length ($l$). The permeate molar fraction in Equations 6-9, $y'$, is the local concentration and varies with length and width ($w$), as for $y$ in Equation 12, it is the average permeate molar fraction, in the main stream, over all the width ($W$), for a given $l$ [49].

The solution proposed by Pan to eliminate the dependence over the width in Equations 6-9 and the existence of a lot of differential equations is presented below [50].

$$\frac{y'}{1-y'} = \frac{\alpha\,(x - \gamma y')}{1 - x - \gamma\,(1-y')} \quad (13)$$

$$\frac{u}{u_f} = \left(\frac{y'}{y'_f}\right)^{[\gamma(\alpha-1)+1]/[(\alpha-1)(1-\gamma)]}\left(\frac{1-y'}{1-y'_f}\right)^{[\gamma(\alpha-1)-\alpha]/[(\alpha-1)(1-\gamma)]}\left(\frac{\alpha-(\alpha-1)y'}{\alpha-(\alpha-1)y'_f}\right) \quad (14)$$

$$2W\frac{L_{p,2}}{d}\frac{P_f}{u_f} = \frac{1}{\alpha(1-\gamma)}\left\{\alpha-(\alpha-1)y'_f - [\alpha-(\alpha-1)y'_f]\frac{u_r}{u_f} - (\alpha-1)\int_{y'_f}^{y'_r}\left(\frac{u}{u_f}\right)_\gamma dy'\right\} \quad (15)$$

Therefore, Equations 10-15 become the governing equations for this model, and the calculation procedure is as follow.

#### *3.3.1.1 Calculation Procedure [49]*

For a given module with fixed membrane dimensions ($L$, $W$, $d$, $t_{\mathrm{p}}$), known operating conditions ($P_{\mathrm{f}}$, $P_{\mathrm{p},0}$, $U_{\mathrm{f}}$, $x_{\mathrm{f}}$) and performance parameters ($L_{\mathrm{p},2}$, $\alpha$), the retentate flow and fraction, $U_r$, $x_r$, at a given $l$, depend only on the permeate/feed pressure ratio ($\gamma$), according to Equations 13-15. This way, the right sides of Equations 10-12 are only functions of $\gamma$. Therefore, with an assumed permeate pressure profile, it is possible to solve all governing equations and obtain the desired profiles.

This leads to an iterative process, and the iteration procedure is as follow:

1) As a first approximation, the permeate pressure is assumed to be equal to $P_{p,0}$ everywhere.
2) By solving the system of Equations 13-15, it is obtained $x_{\mathrm{r}}(l)$, $y'_{\mathrm{r}}(l)$ and $u_{\mathrm{r}}(l)$ profiles.
3) With the profiles determined in the previous step, Equations 10-12 are integrated (where $V = Vy = 0$ in $l = 0$ and $\gamma = P_{\mathrm{p},0}/P_f$ in $l = L$) and the $V(l)$, $Vy(l)$ and $\gamma(l)$ profiles are obtained.
4) The new permeate pressure profile of Step 3 is used in the next iteration.
5) Steps 2-4 are repeated until the permeate pressure profile between successive iterations converges.

The mathematical model and respective calculation procedure were implemented in Scilab 6.0.1 to better understand the flow in a spiral wound membrane and to optimize the membrane design and operating conditions. The code written in this software can be consulted in Appendix 1.

### 3.1.2 Hollow Fiber Membrane

The mathematical formulation for the permeation of a hollow fiber module is simpler than of a SWM, since the fluid flows mainly in one direction in both sides (one-dimensional problem) and there is no significant pressure drop in the permeate or feed/retentate sides. The mathematical model for this module configuration was formulated for the three possible patterns in which HF may operate (co-current, counter-current and cross-flow), as mentioned in Chapter 2.

The following assumptions have been made while formulating and modeling these three systems [51]:

1. The feed stream flows through the inside of the hollow fibers, as the permeate stream flows on the outside.
2. Plug flow is considered.

3. There are no concentration gradients in the perpendicular direction of the membrane.
4. Membrane permeability is constant, independent of pressure and temperature.
5. The total pressure on each side of the membrane is constant.
6. The gas mixture is treated as ideal.
7. Steady state is assumed.
8. All hollow fibers in the module are identical.

According to the above assumptions, the governing equations for a binary mixture in a hollow fiber permeator in counter-current flow are as follows [38]:

Permeation:

$$\frac{\mathrm{d}(Ux)}{\mathrm{d}l} = \frac{\mathrm{d}(U_1)}{\mathrm{d}l} = -N_\mathrm{f} D_\mathrm{ln} \frac{L_{\mathrm{p},1}}{d} \left(P_\mathrm{f} x - P_\mathrm{p} y\right) \tag{16}$$

$$\frac{\mathrm{d}[U(1-x)]}{\mathrm{d}l} = \frac{\mathrm{d}(U_2)}{\mathrm{d}l} = -N_\mathrm{f} D_\mathrm{ln} \frac{L_{\mathrm{p},2}}{d} \left[P_\mathrm{f}(1-x) - P_\mathrm{p}(1-y)\right] \tag{17}$$

$$\frac{\mathrm{d}(Vy)}{\mathrm{d}l} = \frac{\mathrm{d}(V_1)}{\mathrm{d}l} = -N_\mathrm{f} D_\mathrm{ln} \frac{L_{\mathrm{p},1}}{d} \left(P_\mathrm{f} x - P_\mathrm{p} y\right) \tag{18}$$

$$\frac{\mathrm{d}[V(1-y)]}{\mathrm{d}l} = \frac{\mathrm{d}(V_2)}{\mathrm{d}l} = -N_\mathrm{f} D_\mathrm{ln} \frac{L_{\mathrm{p},2}}{d} \left[P_\mathrm{f}(1-x) - P_\mathrm{p}(1-y)\right] \tag{19}$$

Logarithmic mean diameter definition:

$$D_\mathrm{ln} = \frac{\pi \left(d_\mathrm{e} - d_\mathrm{i}\right)}{\ln(d_\mathrm{e}/d_\mathrm{i})} \tag{20}$$

Molar fraction definition:

$$x = \frac{U_1}{U_1 + U_2}, \qquad y = \frac{V_1}{V_1 + V_2} \tag{21}$$

For co-current flow, Equations 18 and 19 have the opposite signal on the right side, since the flow increases with the length. As for the cross-flow pattern, since the direction of the permeate stream has no impact on the separation performance, it was considered equal to the feed stream, for computational reasons [38]. The permeation equations are defined in a similar way as in a spiral wound module (Equations 6 and 7).

The solution of this mathematical model is obtained by solving the system of ODE's presented above, knowing that in $l = 0$, $U_1 = U_\mathrm{f} x_\mathrm{f}$, $U_2 = U_\mathrm{f}(1 - x_\mathrm{f})$ and $V_1 = V_2 = 0$ for co-current and cross-flow. For counter-current flow, the last condition is true in $l = L$.

This mathematical model was also implemented in Scilab 6.0.1, with the same objectives as to the one of spiral wound membrane. The code written to obtain the solution of this model is

reported in Appendix 1, for the three flow patterns studied. In the counter-current code, it was used the shooting method to achieve a flow of zero in $l = L$, since it is not known *a priori* the composition of the permeate stream in $l = 0$.

## 3.2 Experimental Evaluation

### 3.2.1 Membrane selection and information

In order to experimentally evaluate the $O_3/O_2$ separation through a membrane, it was necessary to choose the membrane material that would not degrade with the ozone passage and would be possible to observe a separation of these gases.

According to the information referred in the previous chapter, it was acknowledged that there are several polymers resistant to the high reactivity of the ozone. Between those polymers, the polydimethyl siloxane (PDMS) was the one with sufficient proof that it was capable of separating the oxygen and ozone.

Once the membrane material was selected, it was performed a search for suppliers to acquire a membrane. The suppliers found that better satisfied the requirements presented were PermSelect and SolSep. The selected membrane was a spiral wound module provided by SolSep (Apeldoorn, The Netherlands), see Figure 7. The module dimensions are summarized in Table 5. The membrane was placed inside a pressure vessel with a width of 30 cm and a diameter of 6 cm.

*Figure 7 - Spiral wound module*

*Table 5 - Dimensions of membrane module*

| | |
|---|---|
| **Number of membrane leaves** | 1 |
| **Length of membrane leaf, $L$ / m** | 0.74 |
| **Width of membrane leaf, $W$ / m** | 0.19 |
| **Permeate spacer thickness, $t_p$ / mm** | 1 |
| **Feed/retentate spacer thickness, $t_f$ / mm** | 1 |

### 3.2.2 Installation

The experimental setups, where the membrane module was included, are represented in Figures 8 and 9.

The setup of Figure 8 was used to determine the membrane permeability of pure $O_2$ by feeding pure oxygen to it, where the transmembrane pressure was changed between 0 and 1 barg and correlated to the permeate flow rate measured.

To obtain the membrane permeabilities of ozone and oxygen, in the mixture state, and the $O_3/O_2$ selectivity, it was feed to the membrane a mixture of ozone and oxygen according to the experimental setup of Figure 9. In this case, it was used a sweep gas (helium) in order to create a concentration difference between both sides of the membrane and facilitate the gas permeation, since it was not possible to increase the feed pressure neither realize vacuum in the permeate side. The main reasons for this were, the ozone generator operates at 1 bar, and no compressor or vacuum pump with sealings resistant to ozone exist at the moment in the group. It were realized two different tests were the feed flow rate was altered and, in one, the ozone quantity fed was kept constant and, in the other, it was the ozone concentration.

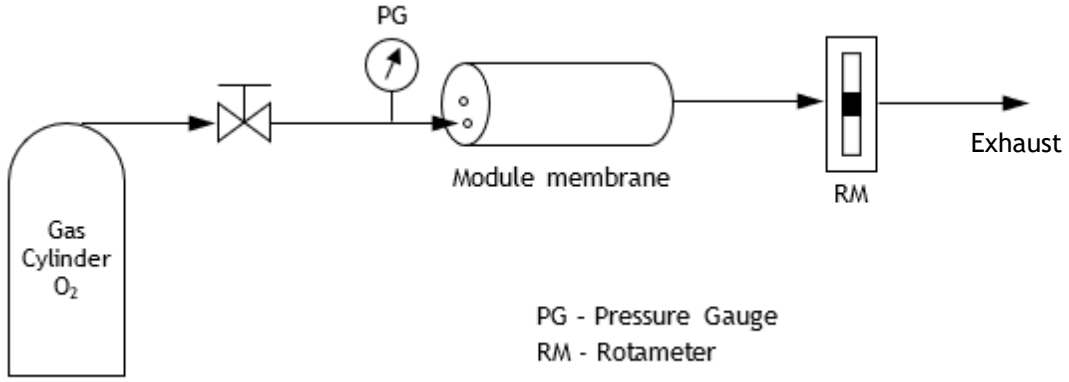


*Figure 8 – Schematics of the experimental setup to determine the $O_2$ permeability*

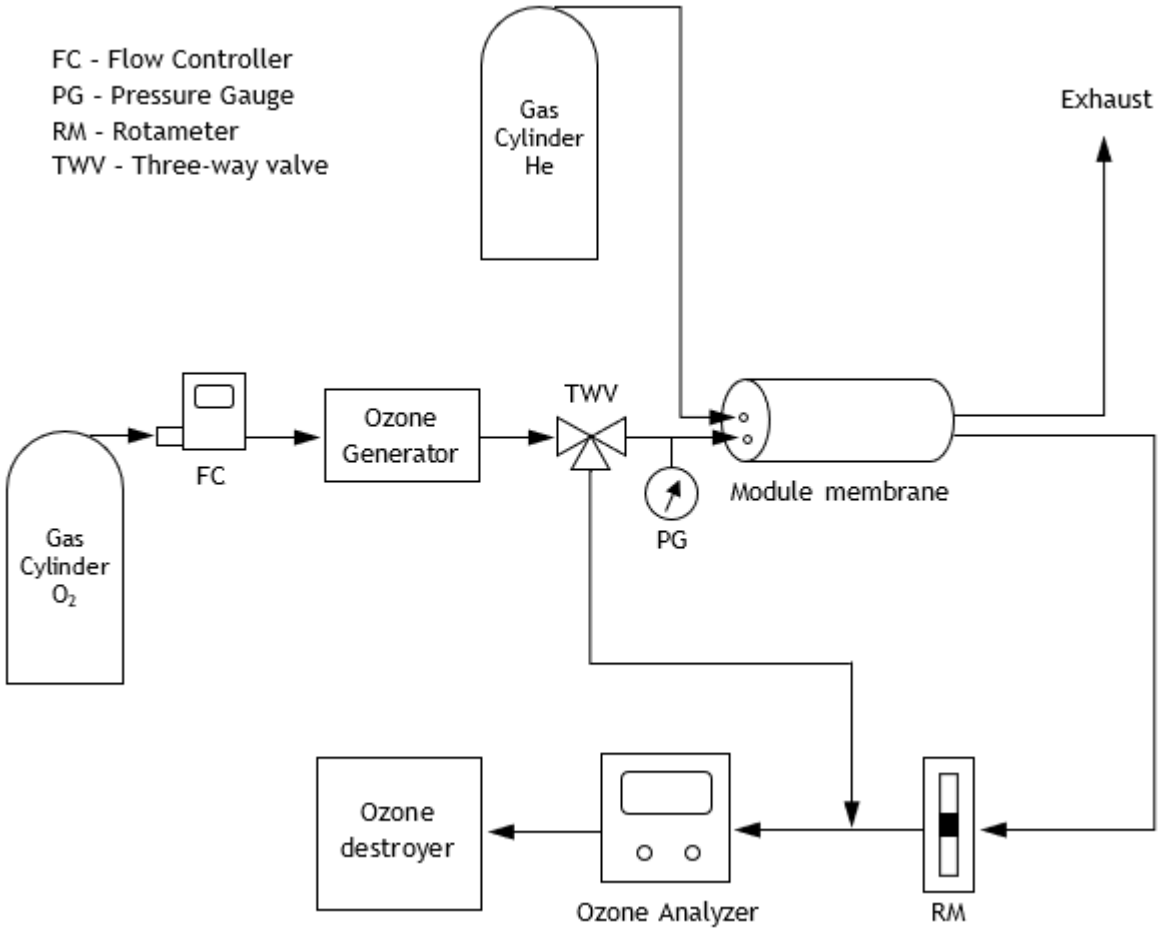


*Figure 9 – Schematics of the experimental setup to determine the $O_3$ permeability*

# 4 Results and Discussion

## 4.1 Mathematical Modeling

### 4.1.1 Spiral Wound Membrane

The mathematical model for SWM referred in the previous chapter was simulated changing from run to run one parameter at a time, keeping the others constant, to evaluate its influence in the output arguments (flow rate, $O_3$ molar fraction and total pressure in the permeate side). The variation of the parameters was made around the values found in the literature and summarized in Table 6.

*Table 6 - Reference data of the simulations [29, 30, 52]*

| | |
|---|---|
| **Length of membrane leaf, $L$ / m** | 1 |
| **Width of membrane leaf, $W$ / m** | 0.3 |
| **Membrane thickness, $d$ / mm** | 0.5 |
| **Permeate spacer thickness, $t_p$ / mm** | 0.25 |
| **Permeability of the spacing material, $B$ / m$^2$** | $3\times10^{-13}$ |
| **Feed side pressure, $P_f$ / bar** | 6 |
| **Permeate outlet pressure, $P_{p,0}$ / bar** | 1 |
| **Feed volumetric flow rate at 1 bar and 25 °C, $Q_f$ / L·min$^{-1}$** | 1 |
| **Feed molar fraction of ozone, $x_f$** | 0.09 |
| **Membrane permeability of $O_2$, $L_{p,2}$ / mol·m·m$^{-2}$·s$^{-1}$·Pa$^{-1}$** | $2.81\times10^{-13}$ |
| **Selectivity, $\alpha$** | 4 |

The value obtained in the literature for the permeability of the spacing materials ($B$) was ~$3\times10^{-10}$ m$^2$ [52]. However, with this value and the data of Table 6, the mathematical model did not show a significant pressure drop in the permeate side, so this parameter was reduced 1000 times to be possible to observe some pressure drop in the parameter analysis. The effect of the membrane and permeate spacer thickness and the feed molar fraction on the membrane flow were not studied, since there is not a large margin of variation of these parameters.

The figures below present all the situations assessed and the units of the parameter in the legends are the same presented in Table 6.

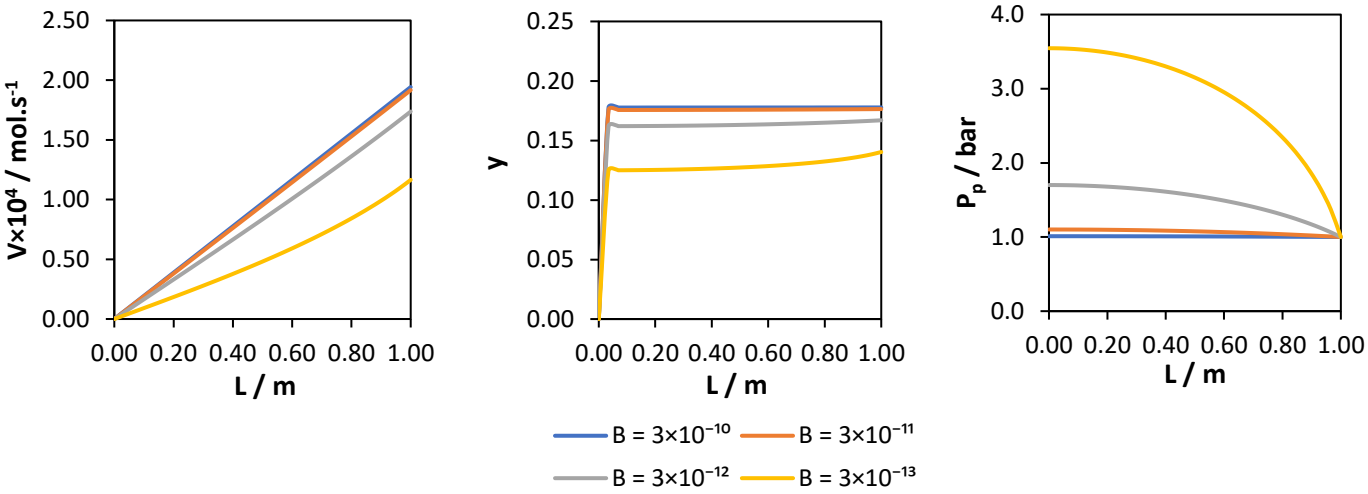


*Figure 10 - Simulation outputs along the membrane length, with parameter $B$ variation*

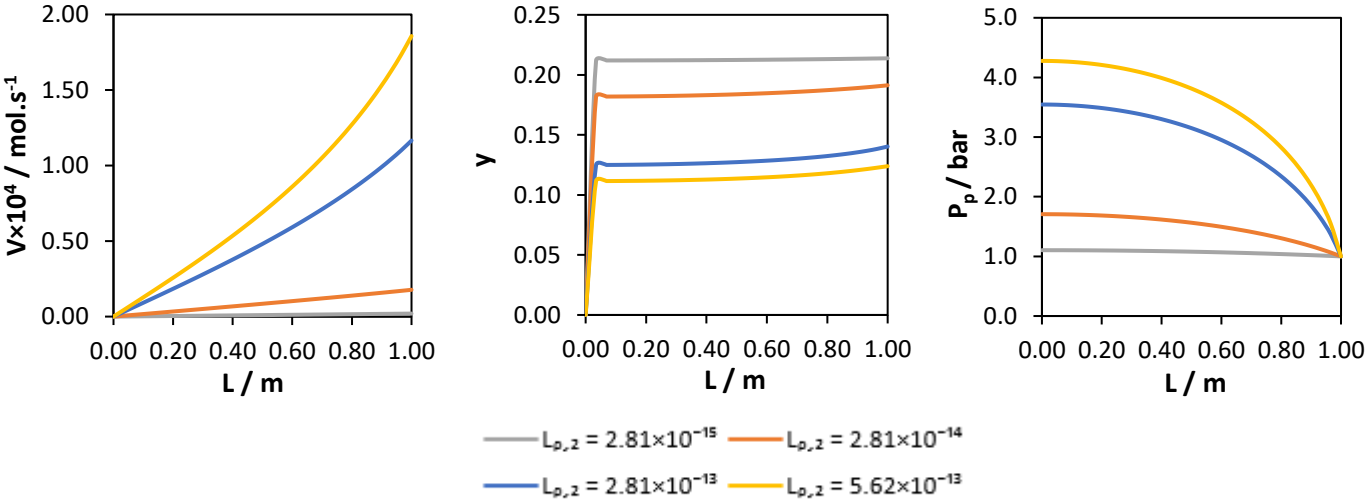


*Figure 11 - Simulation outputs along the membrane length, with membrane permeability of $O_2$ variation*

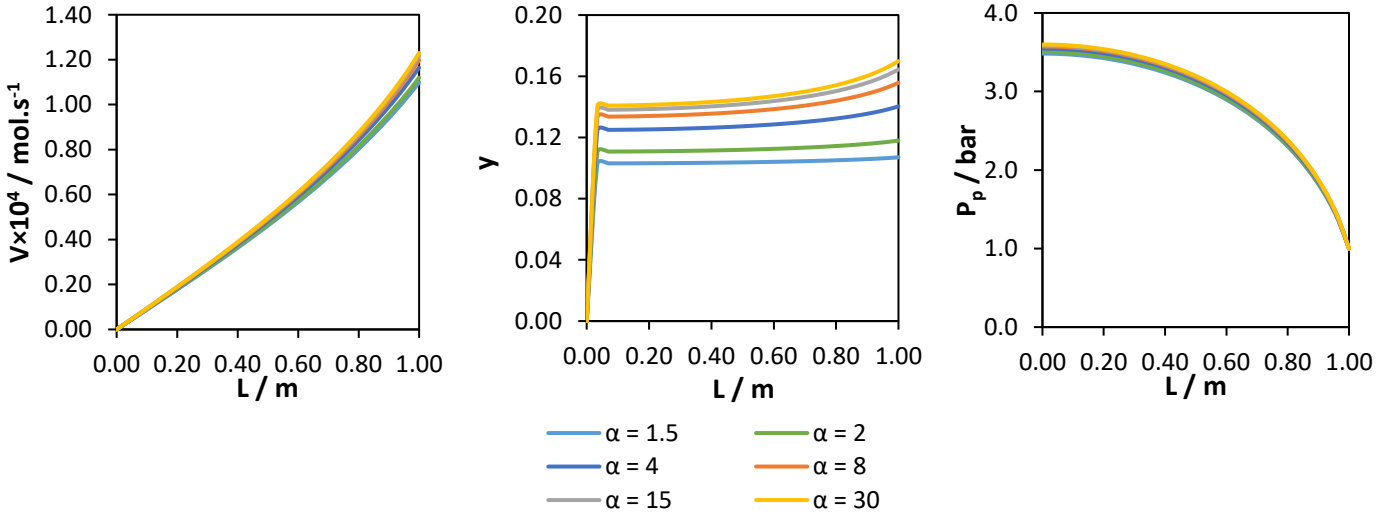


*Figure 12 - Simulation outputs along the membrane length, with selectivity variation*

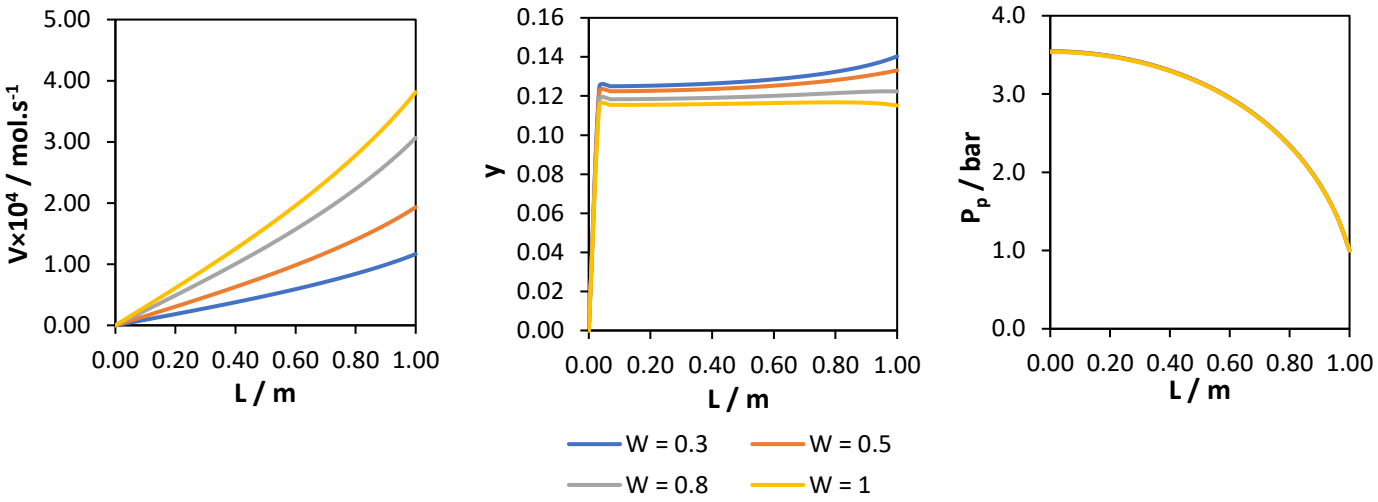


*Figure 13 - Simulation outputs along the membrane length, with width variation*

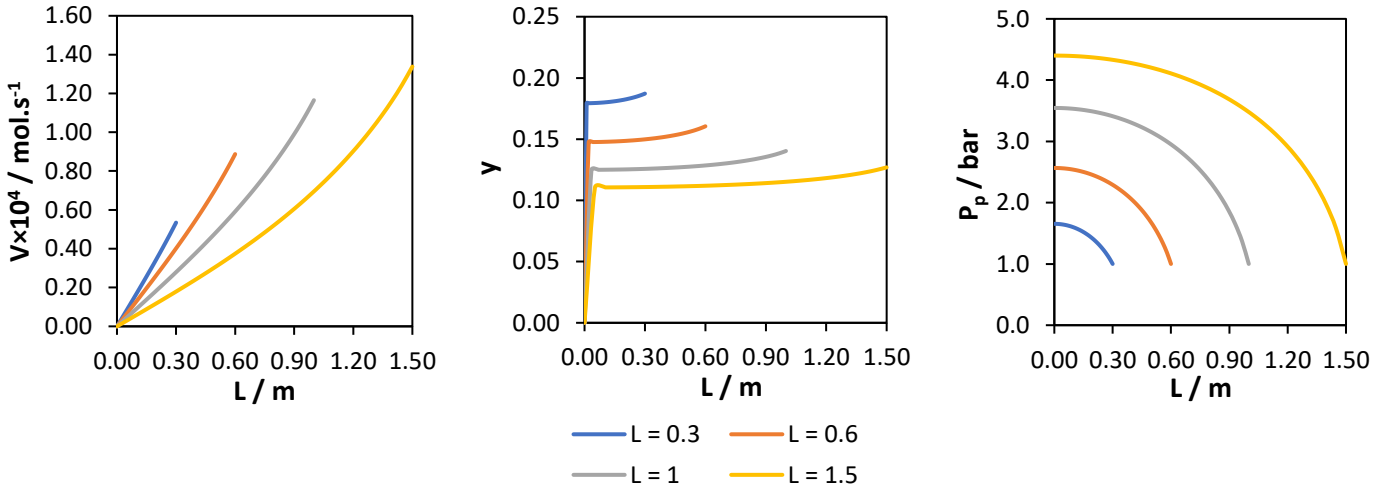


*Figure 14 - Simulation outputs along the membrane length, with length variation*

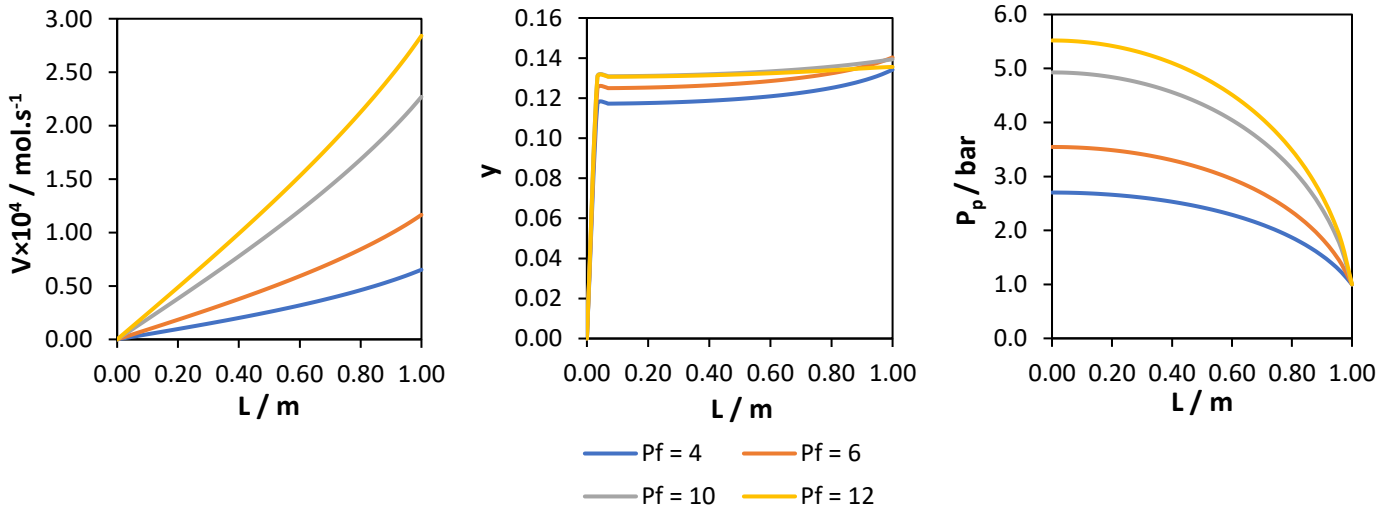


*Figure 15 - Simulation outputs along the membrane length, with feed pressure variation*

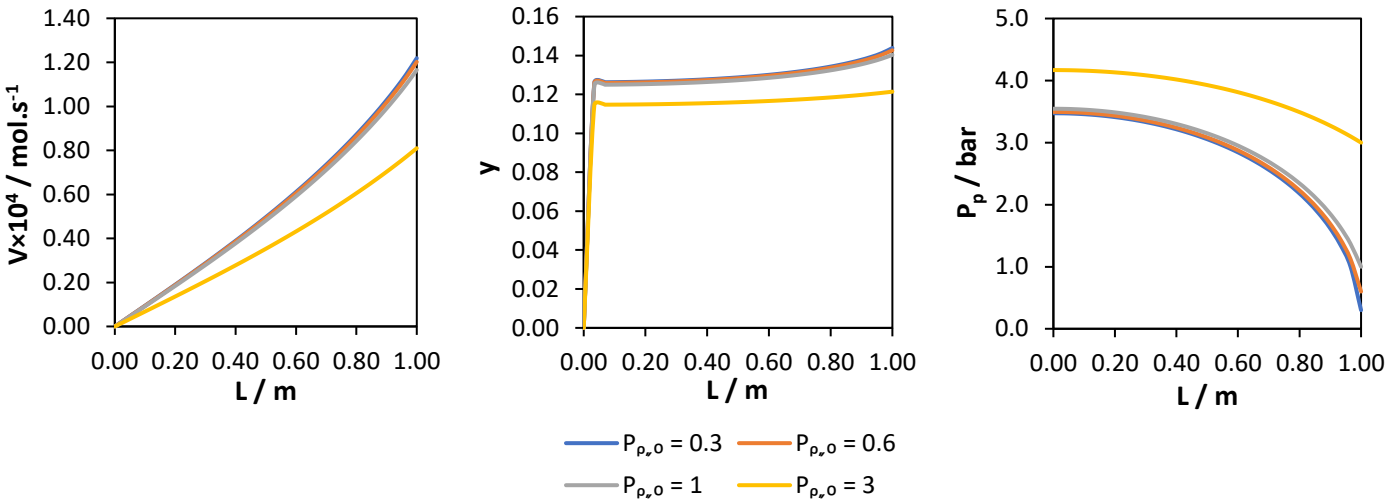


*Figure 16 – Simulation outputs along the membrane length, with permeate pressure outlet variation*

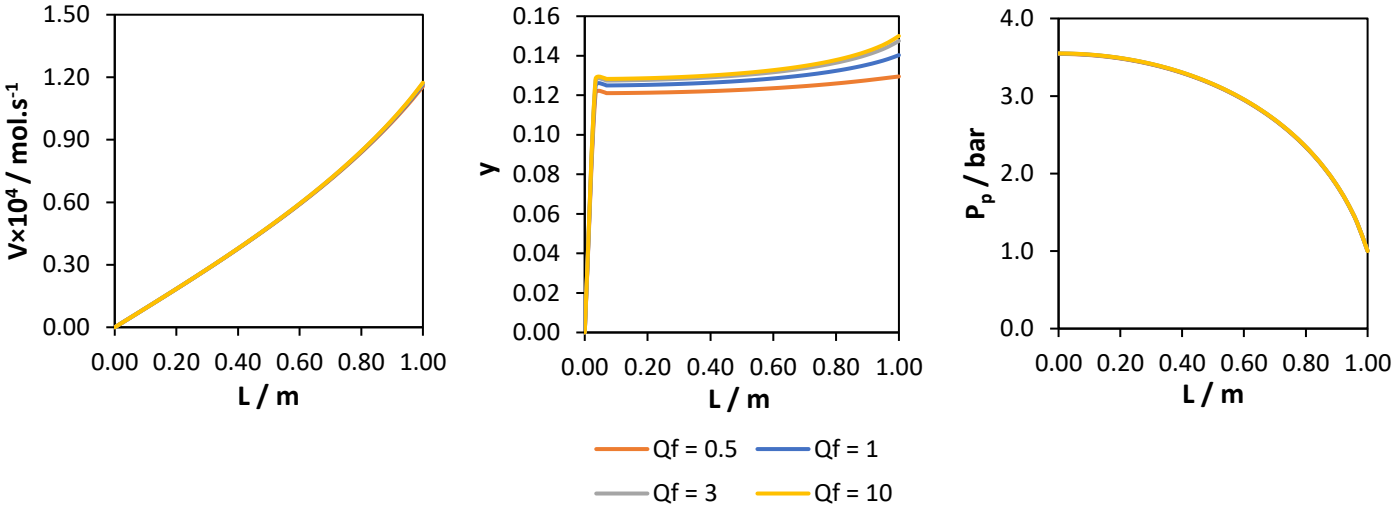


*Figure 17 – Simulation outputs along the membrane length, with feed flow rate variation*

With the reduction of the parameter $B$, it was observed an increase in the permeate pressure drop, explained by the Darcy's law (Equation 10). This causes a decrease in the driving force (Equations 6 and 7), which promotes the decrease of the flow rate and $O_3$ molar fraction in the permeate side.

The variation of the membrane permeability of oxygen affects the permeate flux, according to Equations 6 and 7. So, increasing this parameter increases the total permeate flow rate and, consequently, the pressure drop (Darcy's law). As for the permeate composition, with higher permeability, ozone permeates more through the membrane in the beginning. However, in a given point, it starts to permeate more oxygen than ozone, since the driving force for $O_3$ permeation is too low. So, this component ends up diluted in the $O_2$, observing a decrease in the profiles obtained.

The selectivity affects the membrane affinity towards one component than the other, thereby its variation mainly changes the ozone quantity in the permeate side, keeping the other output parameters mostly constants.

Increasing the membrane width or length, expands the exchange area, increasing the total permeate flow rate. Nevertheless, the ozone composition in the permeate side decreases along the membrane length, for the same reason as in the membrane permeability variation. For the variation of the width, the pressure drop remains the same, given that the right side of Equation 10 does not change significantly (permeate flow rate and width increase or decrease in the same proportion). As for the length variation, the right side of Equation 10 increases, since the only parameter of the expression that varies significantly is the permeate flow rate.

The increasing of the feed pressure facilitates the gas permeation through the membrane since the driving force is higher (Equations 6 and 7). This causes the increase of the flow rate and the pressure drop in the permeate side. The ozone composition also increases, but it is observed a small decrease of the $O_3$ molar fraction close to $l = L$ for higher pressures, which can be explained by the fact that ozone is starting to get diluted in the oxygen, due to ozone starvation in that part of the membrane.

The explanations for the tendencies observed in the permeate outlet pressure vary in a similar way to the ones of the feed pressure variation. In the case of the $O_3$ permeate composition, it decreases with the rise of $P_{\mathrm{p},0}$ along all $l$, given that the driving force is not high enough to promote the ozone permeation for the values studied. With the lower values of pressure analyzed are very close to each other and consequently, it was not observed a big difference between the represented results.

Finally, if the feed flow rate is increased, it does not change much in the studied variables, as observed in Figure 17, since the membrane capacity to permeate continues to be the same and the driving force is kept practically the same. The increasing of the ozone composition in the permeate side might be explained by the fact that the retentate composition becomes almost constant along the membrane and is equal to the feed one (stream flows at a higher velocity).

### 4.1.2 Hollow Fiber membrane

For hollow fiber membranes, it was made a similar parametric study as the one presented previously for spiral wound membranes. The reference values for the parameters analyzed are summarized in Table 7.

*Table 7 - Reference data of the simulations [29, 30]*

| | |
|---|---|
| **Number of fibers, $N_f$** | 80 |
| **Length of membrane module, $L$ / m** | 1 |
| **Internal diameter of each membrane fiber, $d_i$ / mm** | 1 |
| **Fibers thickness, $d$ / mm** | 0.5 |
| **Feed side pressure, $P_f$ / bar** | 6 |
| **Permeate side pressure, $P_p$ / bar** | 1 |
| **Feed volumetric flow rate at 1 bar and 25 °C, $Q_f$ / L·min$^{-1}$** | 1 |
| **Feed molar fraction of ozone, $x_f$** | 0.09 |
| **Membrane permeability of $O_2$, $L_{p,2}$ / mol·m·m$^{-2}$·s$^{-1}$·Pa$^{-1}$** | 2.81×10$^{-13}$ |
| **Selectivity, $\alpha$** | 4 |

The parameters analyzed were the membrane permeability of oxygen, the selectivity, the membrane length, the number of fibers, the feed and permeate pressure, and the feed flow rate. The following figures present the results obtained for each studied parameter in counter-current flow. The results for co-current and cross-flow are summarized in Appendix 2. The parameters units in the graphs legends are the same as the ones in Table 7.

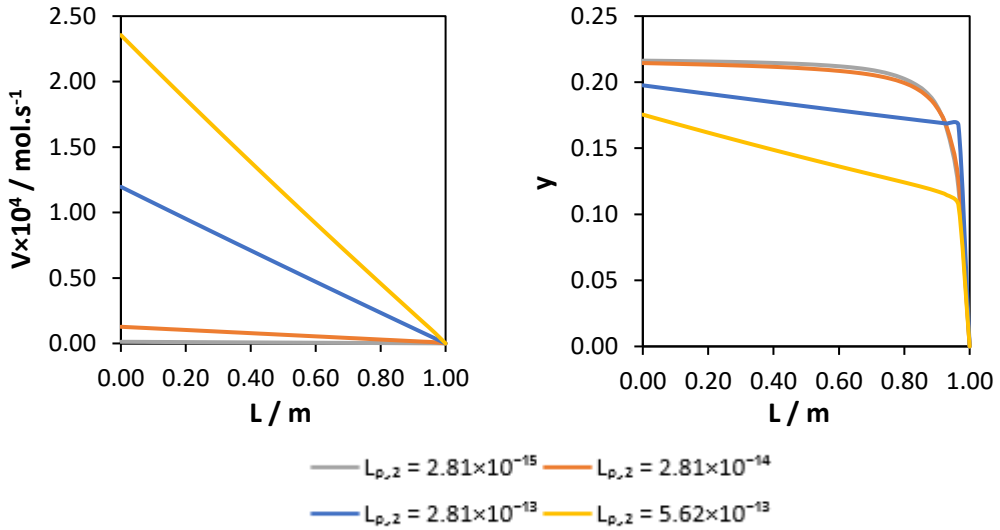


*Figure 18 - Simulation outputs along the membrane length, with membrane permeability of $O_2$ variation*

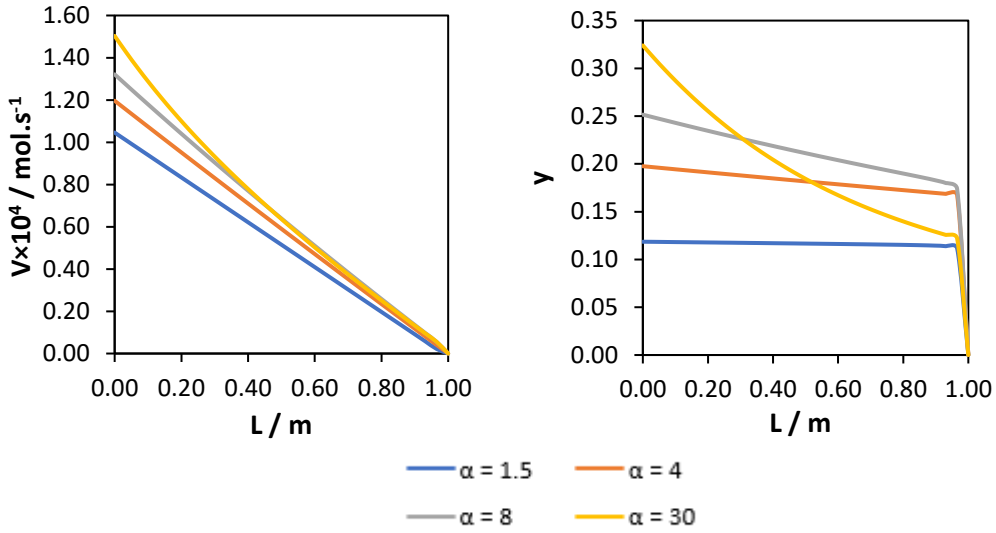


*Figure 19 – Simulation outputs along the membrane length, with selectivity variation*

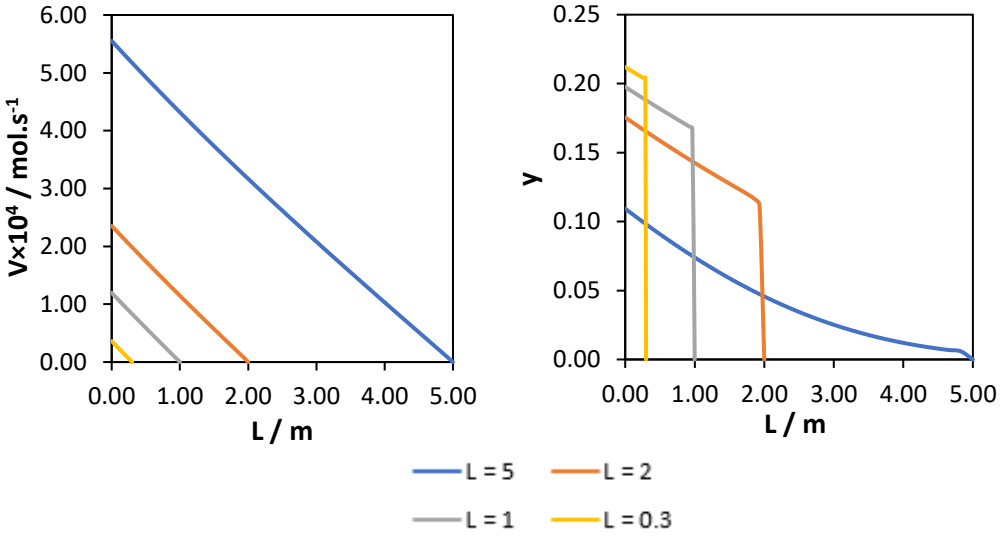


*Figure 20 – Simulation outputs along the membrane length, with length variation*

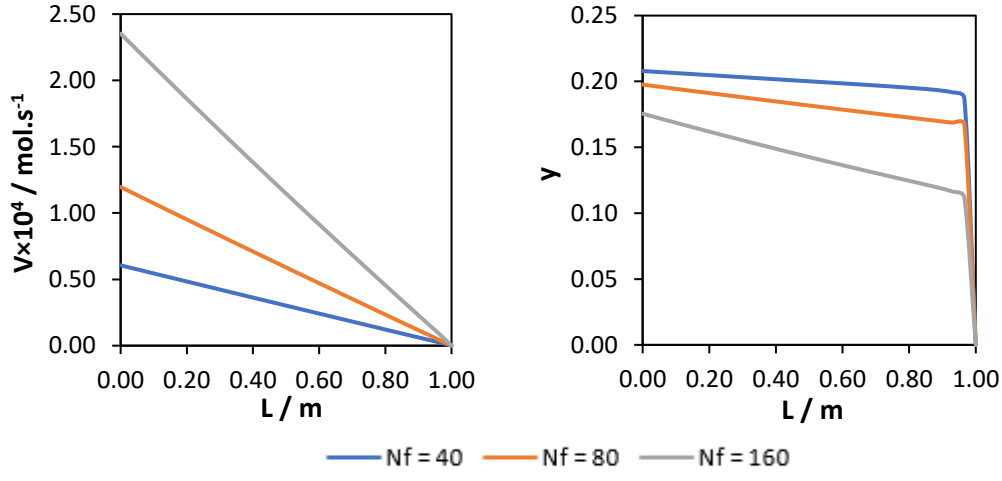


*Figure 21 – Simulation outputs along the membrane length, with number of fibers variation*

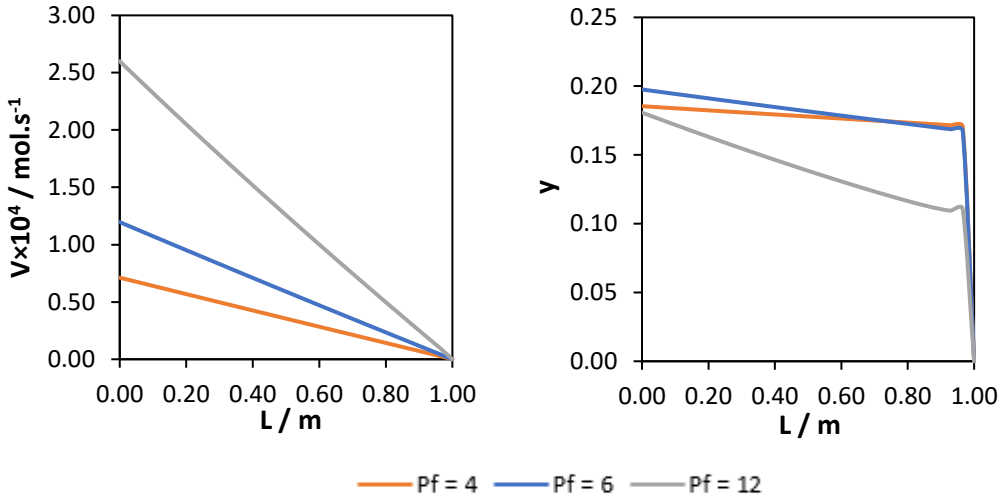


*Figure 22 - Simulation outputs along the membrane length, with feed pressure variation*

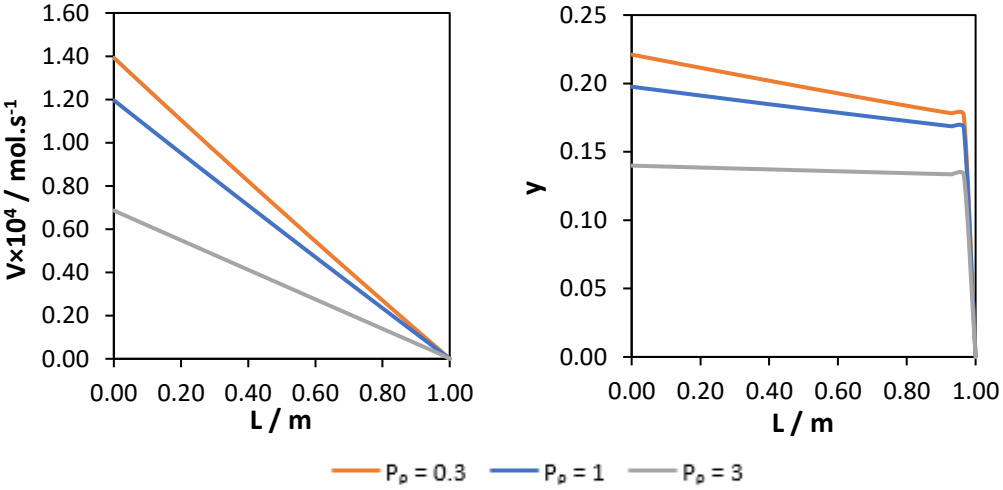


*Figure 23 - Simulation outputs along the membrane length, with permeate pressure variation*

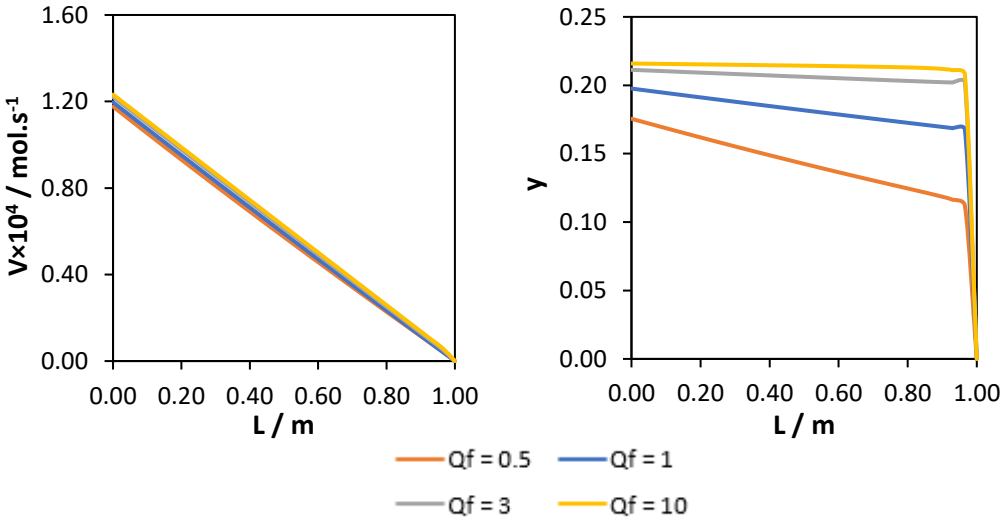


*Figure 24 - Simulation outputs along the membrane length, with feed flow rate variation*

In general it was observed that by increasing the membrane permeability of oxygen, the selectivity, the membrane length, the number of fibers or the feed pressure or decreasing the permeate pressure, the $O_2/O_3$ separation is improved, promoting the increase of the permeate flow rate. The main possible reasons for these tendencies are the increase of the driving force, of the mass transfer area or the enhancement of the membrane performance. However, the ozone composition in the permeate stream decreases in most cases, since the membrane starts at a given point to permeate more oxygen than ozone (ozone starvation), and $O_3$ gets diluted with the $O_2$ that keeps permeating.

In the case of increasing the selectivity, the $O_3$ molar fraction rises, given that the membrane has more affinity to ozone (more permeable) than to oxygen (less permeable). If the selectivity starts to be too high, there is a bigger permeation of ozone close to $l = 0$ (feed/retentate side has more $O_3$ in this zone). Consequently, nearby $l = L$, the oxygen is the one being more permeated, and the ozone becomes diluted, since there is less $O_3$ in the feed/retentate side in this zone.

With the increase of the feed pressure, it is observed an optimum value for this parameter in terms of $O_3$ molar fraction, due to again the ozone starvation.

As for the feed flow rate variation, the tendencies obtained are identical as the ones in the spiral wound membrane and the explanations are also similar – the driving force is the same (permeate flow rate is similar) and the stream flows at a higher velocity (increasing $O_3$ molar fraction).

The parameter analysis obtained for co-current and cross-flow patterns presented similar tendencies to the counter-current flow. The main difference between the three modes is the separation efficiency. To verify which flow pattern is better, it was compiled in a table all the results obtained (flow rate and $O_3$ mass fraction) for each situation studied at the permeate outlet. This table is presented below.

*Table 8 - Permeate outlet data for the three different flow patterns in the parameter analysis*

| | ***Co-current*** | | ***Counter-current*** | | ***Cross-flow*** | |
|---|---|---|---|---|---|---|
| | $V\times10^4$ ($mol\cdot s^{-1}$) | $y$ | $V\times10^4$ ($mol\cdot s^{-1}$) | $y$ | $V\times10^4$ ($mol\cdot s^{-1}$) | $y$ |
| $L_{p,2} = 5.62\times10^{-13}$ | 2.32 | 0.16 | 2.36 | 0.18 | 2.27 | 0.17 |
| $L_{p,2} = 2.81\times10^{-13}$ | 1.19 | 0.19 | 1.15 | 0.20 | 1.16 | 0.20 |
| $L_{p,2} = 2.81\times10^{-14}$ | 0.12 | 0.21 | 0.13 | 0.21 | 0.12 | 0.22 |
| $L_{p,2} = 2.81\times10^{-15}$ | 0.01 | 0.22 | 0.01 | 0.22 | 0.01 | 0.23 |
| $a = 1.5$ | 1.06 | 0.12 | 1.05 | 0.12 | 1.05 | 0.12 |
| $a = 4$ | 1.19 | 0.19 | 1.20 | 0.20 | 1.16 | 0.20 |
| $a = 8$ | 1.27 | 0.23 | 1.32 | 0.25 | 1.24 | 0.25 |
| $a = 30$ | 1.36 | 0.26 | 1.50 | 0.32 | 1.36 | 0.31 |
| $L = 0.3$ | 0.36 | 0.21 | 0.36 | 0.21 | 0.35 | 0.22 |
| $L = 1$ | 1.19 | 0.19 | 1.20 | 0.20 | 1.16 | 0.20 |
| $L = 2$ | 2.32 | 0.16 | 2.35 | 0.18 | 2.27 | 0.17 |
| $L = 5$ | 5.53 | 0.11 | 5.56 | 0.11 | 5.45 | 0.11 |
| $N_f = 40$ | 0.60 | 0.20 | 0.61 | 0.21 | 0.58 | 0.21 |
| $N_f = 80$ | 1.19 | 0.19 | 1.20 | 0.20 | 1.16 | 0.20 |
| $N_f = 160$ | 2.32 | 0.16 | 2.35 | 0.18 | 2.27 | 0.17 |
| $P_f = 4$ | 0.71 | 0.18 | 0.71 | 0.19 | 0.68 | 0.19 |
| $P_f = 6$ | 1.19 | 0.19 | 1.20 | 0.20 | 1.16 | 0.20 |
| $P_f = 12$ | 2.58 | 0.17 | 2.60 | 0.18 | 2.55 | 0.18 |
| $P_p = 0.3$ | 1.39 | 0.22 | 1.39 | 0.22 | 1.38 | 0.22 |
| $P_p = 1$ | 1.19 | 0.19 | 1.20 | 0.20 | 1.16 | 0.20 |
| $P_p = 3$ | 0.68 | 0.14 | 0.69 | 0.14 | 0.62 | 0.15 |
| $Q_f = 0.5$ | 1.16 | 0.16 | 1.18 | 0.18 | 1.14 | 0.17 |
| $Q_f = 1$ | 1.19 | 0.19 | 1.20 | 0.20 | 1.16 | 0.20 |
| $Q_f = 3$ | 1.21 | 0.21 | 1.22 | 0.21 | 1.17 | 0.22 |
| $Q_f = 10$ | 1.22 | 0.22 | 1.23 | 0.22 | 1.18 | 0.22 |

Overall, counter-current flow showed a higher flow rate and $O_3$ molar fraction, on the permeate outlet, than co-current, *i.e.*, it has a higher separation efficiency. The cross-flow pattern exhibited similar ozone compositions to counter-current, but lower flow rates. There were a few exceptions that might be due to the low accuracy of the shooting method used in the counter-current simulations.

As mentioned in Chapter 2, counter-current flow is the more efficient flow pattern of all the three, since it gives higher flow rates and ozone molar fractions. Co-current provides the lowest ozone fractions, being the less efficient flow configuration.

Another difference between the three patterns is the variation of the $O_3$ molar fraction along the membrane length in the fluid flow direction, which increases, in counter-current, and decreases, in co-current and cross-flow. This predisposition happens according to the ozone quantity in the feed/retentate side.

## 4.2 Experimental data

Results of the preliminary experimental tests to determine the membrane permeability of the gases in study in the SWM are presented first for pure oxygen (Figure 25) and then for binary mixture of ozone and oxygen (Table 9). The experimental data of Table 9 does not have into account the flow rate of the sweep gas, the material balances were made only in terms of $O_2$ and $O_3$ (calculations made are described in Appendix 3), since it was considered that helium does not permeate in the opposite way of the permeation in a SWM. The flow rate of this gas was 0.5 $L \cdot min^{-1}$ and the transmembrane pressure was considered equal to 1 bar for all the assays made.

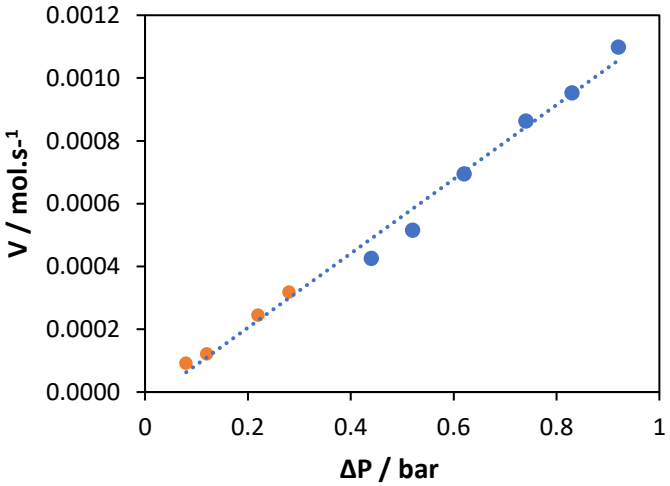


*Figure 25 - Permeate flow rate for different transmembrane pressures*

*Table 9 - Experimental data in the ozone tests*

| Feed | | Retentate | | Permeate | |
|---|---|---|---|---|---|
| $U_f \times 10^4$ (mol·s$^{-1}$) | $x_f$ | $U_r \times 10^4$ (mol·s$^{-1}$) | $x_r$ | $V \times 10^4$ (mol·s$^{-1}$) | $y$ |
| 4.40 | 0.04 | 3.16 | 0.04 | 1.24 | 0.05 |
| 3.67 | 0.05 | 2.52 | 0.05 | 1.15 | 0.06 |
| 2.94 | 0.06 | 1.88 | 0.06 | 1.05 | 0.08 |
| 2.20 | 0.08 | 1.34 | 0.07 | 0.86 | 0.11 |
| 3.67 | 0.05 | 2.49 | 0.05 | 1.18 | 0.06 |
| 2.94 | 0.05 | 1.88 | 0.05 | 1.05 | 0.06 |
| 2.20 | 0.05 | 1.34 | 0.05 | 0.86 | 0.06 |

For the experiment with only oxygen, the flow rate was measured with two different rotameters, one with a range of 0.4-5.0 L·min$^{-1}$ and the other of 0.0-0.5 L·min$^{-1}$, since for small transmembrane pressures, the first rotameter referred was not able to measure the permeate flow rate. Those points are highlighted in different colors in Figure 25.

So, according to Equation 1, the ratio of the membrane permeability to the membrane thickness (membrane permeance) was determined by the slope of the graph presented above (Figure 25), giving a value of $8.45\times10^{-8}$ mol·m$^{-2}$·s$^{-1}$·Pa$^{-1}$.

As for the experiment with a mixture of ozone and oxygen, the membrane permeance was determined from only one point, since it was not possible to change the transmembrane pressure or the flow rate of the sweep gas. Thus, the membrane permeance was equal to $8.84\times10^{-9}$ mol·m$^{-2}$·s$^{-1}$·Pa$^{-1}$ for ozone and $7.47\times10^{-9}$ mol·m$^{-2}$·s$^{-1}$·Pa$^{-1}$ for oxygen. The $O_3/O_2$ ideal selectivity was equal to 1.2, which shows that this membrane is capable of separating oxygen and ozone and it has a higher affinity to ozone, as expected. As for the ideal selectivity, it was obtained a value of 1.4.

As for the experimental tests realized, with the increase of the feed flow rate, the permeate flow rate was supposed to be the same and the $O_3$ molar fraction would increase, according to the simulations made. However, it was measured flow rates a little bit different from each other and the ozone concentration in the permeate flow only changed with the variation of the $O_3$ concentration in the feed stream. This fact might be due to the simulations were performed assuming a higher selectivity than the experimental one, and the range of feed flow rates simulated are from 0.5 to 10 L·min$^{-1}$, while experimentally was tested between 0.3 and 0.6 L·min$^{-1}$. So, for that matter, it was realized a new simulation with a smaller selectivity (around 1.3) and in a range of lower feed flow rates (between 0.2 and 0.5 L·min$^{-1}$), presented in Figure 26. The other parameters were kept equal to the ones in Table 6, for simplicity, since what matters are the tendencies obtained.

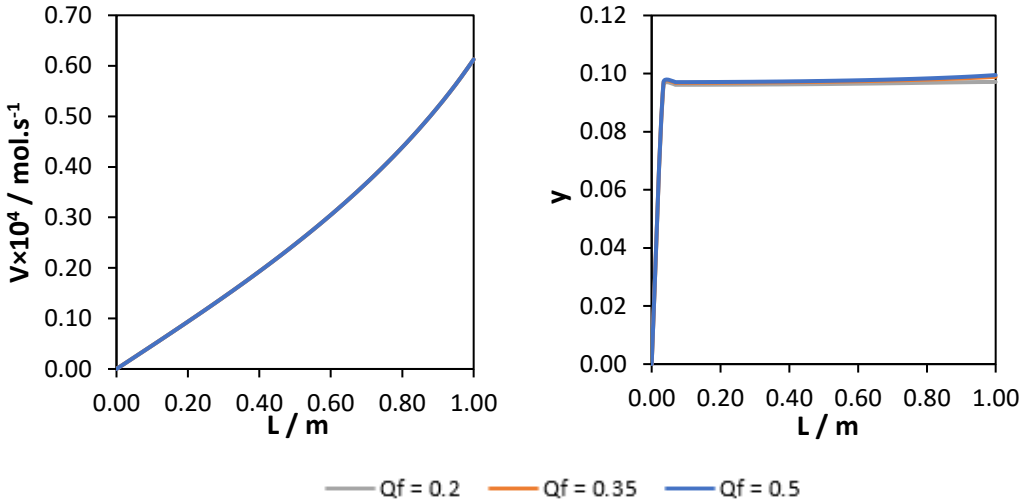


*Figure 26 – Simulation outputs along the membrane length, for small feed flow rates*

According to Figure 26, the permeate flow rate should be constant, regardless of the feed flow rate (low or high). The difference between the experimental data and the simulation tendencies may be explained by the fact that it was observed some oscillations in the flow rate measurement, creating errors in the values registered. As for the ozone composition in the permeate stream, it is in agreement with the simulation tendency. This may be because the membrane might had already reached its minimum permeation capability.

It was also made the same previous simulation with the variation of the ozone composition and a small feed flow rate (0.5 L·min$^{-1}$), see Figure 27.

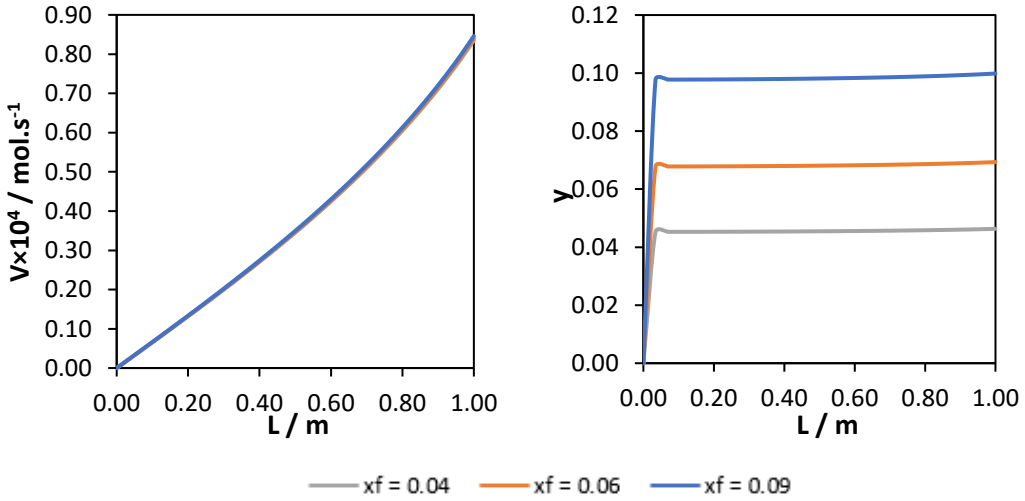


*Figure 27 – Simulation outputs along the membrane length, for different ozone feed molar fractions*

By increasing the ozone concentration in the feed stream, the quantity of $O_3$ would be higher and so, it permeates more ($O_3$ molar fraction is higher in the permeate flow), according to Figure 27. In the experiment realized, it was increased the $O_3$ concentration and decreased the feed flow rate. However, the variation of the feed flow rate does not affect significantly the outlet permeate composition, as seen in Figure 26 and discussed above. As for the ozone concentration variation in the feed stream, it promotes the increase of the $O_3$ molar fraction in the permeate, as expected by the simulation made (Figure 27).

# 5 Conclusion

In this work, the separation of ozone and oxygen was first studied based on the mathematical models, for two different membrane configurations (spiral wound and hollow fiber) and their possible operating flow patterns (co-current, counter-current and cross-flow), with the aim of better understanding the fluid flow in these modules. The results showed that, regardless of the membrane geometry and the flow pattern, the parameters variation generates similar tendencies of the studied variables (flow rate and $O_3$ molar fraction in the permeate stream). This is explained by the fact that a gas separation in a membrane is mainly described by the same generic equation (Equation 1). This is the only comparison that can be made between these two membrane configurations since they do not have a lot in common.

In the mathematical model for the hollow fiber membrane, it was verified that the counter-current flow is more efficient than the co-current and cross-flow patterns, as expected. Nevertheless, the differences between the three of them were not substantial (maximum difference of 0.01-0.02 in the ozone permeate molar fraction and 0.1-0.2 $mol \cdot s^{-1}$ in the permeate outlet flow rate).

Overall, it was concluded that by increasing the membrane permeability of oxygen or ozone, the selectivity, the membrane dimensions or the feed pressure or decreasing the permeate pressure, it is possible to improve, in most of the cases, a gas separation through a membrane. However, the quantity of ozone in the permeate stream may not be as high as desired. So, it is necessary to find a balance between all the studied parameters according to the objective of the separation product.

Regardless of the flow pattern or the membrane geometry adopted, in the simulations made, it was verified that it is possible to enriched between 0.03-0.10, in terms of molar fraction, the ozone concentration in the permeate stream.

The $O_3/O_2$ separation was also studied experimentally in a PDMS spiral wound membrane. To characterize this separation, it was determined the membrane permeance of each of the gases and selectivity. The membrane permeance of pure oxygen and in a mixture with ozone was determined, giving $8.45 \times 10^{-8}$ $mol \cdot m^{-2} \cdot s^{-1} \cdot Pa^{-1}$ and $7.47 \times 10^{-9}$ $mol \cdot m^{-2} \cdot s^{-1} \cdot Pa^{-1}$, respectively. As for ozone, this ratio was only obtained in the mixture state and has a value of $8.84 \times 10^{-9}$ $mol \cdot m^{-2} \cdot s^{-1} \cdot Pa^{-1}$. The $O_3/O_2$ selectivity was found to be about 1.3. With the values found, it was concluded that the spiral wound membrane acquired is capable of separating the $O_3$ and $O_2$, having a higher affinity to ozone, as expected.

# 6 Assessment of the work done

## 6.1 Objectives Achieved

The objectives proposed in the introduction section were all achieved. However, due to the short time available, it was not possible to better validate the mathematical model for SWM with the experimental data obtained, to realize more tests with the membrane acquired and to obtain other types of membranes, in terms of materials and geometries, to better analyze the $O_3/O_2$ separation experimentally.

## 6.2 Limitations and Future Work

The main limitation of this work was to find and understand the mathematical model for a spiral wound membrane and then to implement it in Scilab 6.0.1 that would allow its simulation.

Another limitation was the time spent by using the shooting method to simulate the flow in a hollow fiber module with counter-current flow and its low accuracy.

It was also a problem the time spent to acquire a membrane to verify the ozone and oxygen separation experimentally.

In future work, it would be interesting to evaluate the $O_3/O_2$ separation experimentally again in the spiral wound membrane used in this work with an upgraded installation and a compressor or a vacuum pump, and also in other membrane geometries, such as hollow fiber, and other membrane materials, like PTFE, PVDF, PP (polymers compatible with ozone), ceramics, or mixed matrix membranes, as suggested of PDMS with silicalite-1. It would also be interesting to determine the membrane permeability of helium in the spiral wound membrane acquired or find a way to also determine the quantity of oxygen in the retentate or permeate stream, to verify if it was valid the assumption made in the calculations of this work (helium does not permeate and so only appears in the permeate stream composition).

## 6.3 Final Assessment

This work allowed me to consolidate the knowledge that I acquired over these last five years, mainly of the following curricular units: Separation Processes II, Transfer Phenomena I and Transfer Operations, and to learn that everything in engineering is connected and has very similar basic principles.

It also allowed me to learn more about membrane separations and programming language in Scilab.

# References


1. Camel, V. and A. Bermond, *The use of ozone and associated oxidation processes in drinking water treatment*. Water Research, 1998. **32**(11): p. 3208-3222.
2. handbook, S.s.d.w. *Applications in drinking water treatment*. 2015; Available from: https://www.suezwaterhandbook.com/processes-and-technologies/oxidation-disinfection/oxidation-and-disinfection-using-ozone/applications.
3. Jackson, P.J., G.R. Dillon, T.E. Irving, and G. Stanfield, *Manual on Treatment for Small Water Supply Systems*. 2015, Department of the Environment, Transport and the Regions. p. 95.
4. Information, N.C.f.B. *Ozone*. 2019; Available from: https://pubchem.ncbi.nlm.nih.gov/compound/24823.
5. Loeb, B., C. M. Thompson, J. Drago, H. Takahara, and S. Baig, *Worldwide Ozone Capacity for Treatment of Drinking Water and Wastewater: A Review*. Vol. 34. 2012. 64-77.
6. Gottschalk, C., J. Libra, and A. Saupe, *Ozonation of Water and Waste Water: A Practical Guide to Understanding Ozone and its Applications*. 2nd ed. 2010: Wiley-VCH. 362.
7. Su, M.-C. and N.-H. Kao, *Kinetic Study of Pressurized Ozonation Reactor of Tap Water*. Vol. 4. 2009. 1-10.
8. Wang, L.K., L. Kurylko, and M.H.S. Wang, *Gas dissolving system and method*, in *Google Patents*. 1991.
9. Cook, G.A., A.D. Kiffer, C.V. Klumpp, A.H. Malik, and L.A. Spence, *Separation of Ozone from Oxygen by a Sorption Process*, in *Ozone Chemistry and Technology*. 1959, American Chemical Society. p. 44-52.
10. Fitch, F.R. and A. Maheshwary, *Methods for separating ozone*, in *Google Patents*. 2017.
11. Streng, A.G., *Tables of Ozone Properties*. Journal of Chemical & Engineering Data, 1961. **6**(3): p. 431-436.
12. Lenntech. *Ozone decomposition*. 2019; Available from: https://www.lenntech.com/library/ozone/decomposition/ozone-decomposition.htm.
13. Technologies, O. *Ozone Solubility in water*. 2017; Available from: https://www.oxidationtech.com/ozone/solubility.html.
14. Wei, C.-H., Z. Fengzhen, Y. Hu, C. Feng, and H. Wu, *Ozonation in water treatment: The generation, basic properties of ozone and its practical application*. Vol. 33. 2017.
15. Lenntech. *Ozone toxicology*. 2019; Available from: https://www.lenntech.com/library/ozone/toxicology/ozone-toxicology.htm.
16. Solutions, O. *Ozone Applications*. 2019; Available from: https://www.ozonesolutions.com/journal/ozone-applications/.

17. *Ozone in Water Treatment: Application and Engineering*. 1st ed, ed. B. Langlais, D.A. Reckhow, and D.R. Brink. 1991: Lewis Publishers. 569.
18. Rakness, K.L., *Ozone in Drinking Water Treatment: Process Design, Operation, and Optimization*. 1st ed. 2005: American Water Works Association. 305.
19. Eliasson, B., M. Hirth, and U. Kogelschatz, *Ozone Synthesis From Oxygen in Dielectric Barrier Discharges*. Vol. 20. 2000. 1421.
20. Izumi, J., A. Yasutake, N. Tomonaga, H. Tsutaya, and N. Ok, *Development on High Performance Gas Separation Process Using Gas Adsorption*. Vol. 39. 2002.
21. Fitch, F.R. and S. Finley, *Methods for producing ozone*, in *Google Patents*. 2015.
22. Ferrell, R.J., W. Ji, and P.J. Sadkowski, *Ozone purification*, in *Google Patents*. 2000.
23. Grenier, M. and P. Petit, *Ozone-producing process*, in *Google Patents*. 1988.
24. Izumi, J., A. Yasutake, N. Tomonaga, and H. Tsutaya, *Apparatus for manufacturing high concentration ozone gas*, in *Google Patents*. 2003.
25. Kerry, F.G., *Industrial Gas Handbook: Gas Separation and Purification*. 1st ed. 2007: CRC Press. 581.
26. Janknecht, P., P.A. Wilderer, C. Picard, and A. Larbot, *Ozone–water contacting by ceramic membranes*. Separation and Purification Technology, 2001. **25**(1): p. 341-346.
27. Picard, C., A. Larbot, J. Sarrazin, P. Janknecht, and P. Wilderer, *Ceramic membranes for ozonation in wastewater treatment*. Vol. 26. 2001. 13-22.
28. Santos, F., C. Borges, and F. da Fonseca, *Polymeric Materials for Membrane Contactor Devices Applied to Water Treatment by Ozonation*. Vol. 18. 2015. 1015-1022.
29. Berry, M., C. Taylor, W. King, J. Chew, and J. Wenk, *Modelling of Ozone Mass-Transfer through Non-Porous Membranes for Water Treatment*. Vol. 9. 2017. 452.
30. V. Shanbhag, P. and K. Sirkar, *Ozone and Oxygen permeation behavior of silicone capillary membranes employed in membrane ozonators*. Vol. 69. 1998. 1263-1273.
31. Pines, D., K.-N. Min, S. J. Ergas, and D. Reckhow, *Investigation of an Ozone Membrane Contactor System*. Vol. 27. 2005. 209-217.
32. Ji, W., R.J. Ferrell, and A.I. Shirley, *Ozone purification process*, in *Google Patents*. 2001.
33. Chung, T.-S., L.Y. Jiang, Y. Li, and S. Kulprathipanja, *Mixed matrix membranes (MMMs) comprising organic polymers with dispersed inorganic fillers for gas separation*. Progress in Polymer Science, 2007. **32**(4): p. 483-507.
34. Suen, S.-Y., *Mixed Matrix Membranes for Adsorption Application*. Vol. 6. 2015.
35. Duval, J.M., B. Folkers, M.H.V. Mulder, G. Desgrandchamps, and C.A. Smolders, *Adsorbent filled membranes for gas separation. Part 1. Improvement of the gas separation properties of polymeric membranes by incorporation of microporous adsorbents*. Journal of Membrane Science, 1993. **80**(1): p. 189-198.

36. Tantekin-Ersolmaz, B., C. Atalay-Oral, M. Tather, A. Erdem-Senatalar, B. Schoeman, and J. Sterte, *Effect of zeolite particle size on the performance of polymer–zeolite mixed matrix membranes*. Journal of Membrane Science, 2000. **175**(2): p. 285-288.
37. Mulder, M., *Basic principles of membrane technology*. 2nd ed. 1996: Klower Academic Publishers. 564.
38. Yang, D., H. Ren, Y. Li, and Z. Wang, *Suitability of cross-flow model for practical membrane gas separation processes*. Chemical Engineering Research and Design, 2017. **117**: p. 376-381.
39. Scott, K., *Handbook of Industrial Membranes*. 2nd ed. 1995, Amsterdam: Elsevier Science. 912.
40. Sridhar, S., S. Bee, and S. Bhargava, *Membrane-based Gas Separation: Principle, Applications and Future Potential*. Vol. 2014. 2014.
41. Marriot, J.I., *Detailed modelling and optimal design of membrane separation systems*, PhD thesis, in Department of Chemical Engineering, University College London, 2001.
42. Filtration, S. *Module Configurations & Processes*. 2019; Available from: http://synderfiltration.com/learning-center/articles/module-configurations-process/.
43. Technology, S. *Membrane Based Steviol Glycoside Purification Technology*. Available from: https://www.steviashantanu.com/stevia-membrane-based-extraction.
44. Pandey, P. and R.S. Chauhan, *Membranes for gas separation*. Progress in Polymer Science, 2001. **26**(6): p. 853-893.
45. Marques, C., *Membrane process for carbon capture*, Master Thesis, in Department of Chemical Enginnering, Faculty of Engineering of the University of Porto, 2014.
46. Welty, J.R., C.E. Wicks, R.E. Wilson, and G.L. Rorrer, *Fundamentals of Momentum, Heat, and Mass Transfer*. 5th ed. 2008: John Wiley & Sons, Inc. 740.
47. Qi, R. and M. A. Henson, *Modeling of Spiral-Wound Permeators for Multicomponent Gas Separations*. Vol. 36. 1997.
48. Gu, B., X.Y. Xu, and C.S. Adjiman, *A predictive model for spiral wound reverse osmosis membrane modules: The effect of winding geometry and accurate geometric details*. Computers & Chemical Engineering, 2017. **96**: p. 248-265.
49. Pan, C.Y., *Gas separation by permeators with high-flux asymmetric membranes*. AIChE Journal, 1983. **29**(4): p. 545-552.
50. Pan, C.Y. and H.W. Habgood, *Gas separation by permeation Part I. Calculation methods and parametric analysis*. The Canadian Journal of Chemical Engineering, 1978. **56**(2): p. 197-209.
51. Ahsan, M. and A. Hussain, *Mathematical modelling of membrane gas separation using the finite difference method*. Pacific Science Review A: Natural Science and Engineering, 2016. **18**(1): p. 47-52.

52. Koutsou, C.P., A.J. Karabelas, and T.B. Goudoulas, *Characteristics of permeate-side spacers of spiral wound membrane modules*. Desalination, 2013. **322**: p. 131-136.

# Appendix 1 Scilab Codes

## A1.1 Spiral Wound Membrane

```
clear
global W L P P0 T R Uf uf xf gama QO2_d d sel tp B visc_O3 visc_O2 pts
W = 0.3; L = 1; d = 0.0005 // m
P = 6*10^5 // Pa - alimentação; P0 = 3*10^5 // Pa - permeado
T = 273.15+25 // K; R = 8.314 // m3 Pa/mol K

Qent = (1*10^-3)/(P*10^-5*60) // m3/s
Uf = (P*Qent)/(R*T) // mol/s; uf = Uf/L // mol/s.m
xf = (0.13/(3*16))/(0.13/(3*16)+0.87/(2*16)) // fração molar O3 à entrada

QO2_d = (2.81*10^-13)/d // mol/m2 s Pa
sel = 4

tp = 0.00025 // m; B = 2.9*10^-13 // m2
visc_O3 = 1.5*10^-5; visc_O2 = 2.055*10^-5 // Pa s
const = (-R*T)/(W*tp*B)
pts=30

for u=1:pts
   gama(u)=1
   gama_novo(u)=P0/P
   z(u)=(L/(pts-1))*(u-1) // posição de cada ponto
end

erro=abs(gama-gama_novo); soma=sum(erro)/pts

while soma > 0.0001
   for i=1:pts
      gama(i)=gama_novo(i)
      gama_temp=gama(i)

      yf(i)=(1+(sel-1)*(gama(i)+xf)-sqrt(((1+(sel-1)*(gama(i)+xf))^2)-(4*gama(i)*sel*(sel-
1)*xf)))/(2*gama(i)*(sel-1))
      yf_temp=yf(i)

      f_yf(i)=((yf(i)/yf(i))^((gama(i)*(sel-1)+1)/((sel-1)*(1-gama(i)))))*(((1-yf(i))/(1-yf(i)))^((gama(i)*(sel-
1)-sel)/((sel-1)*(1-gama(i)))))*((sel-(sel-1)*yf(i))/(sel-(sel-1)*yf(i)))
      f_yf_temp=f_yf(i)

      yr_arb=yf_temp-0.01

      function f=fex(y)
      global f_yr_arb h y1 y2 y3 y4 f_y1 f_y2 f_y3 f_y4
      f_yr_arb=((y./yf_temp).^((gama_temp*(sel-1)+1)./((sel-1)*(1-gama_temp))))*(((1-y)./(1-
yf_temp)).^((gama_temp*(sel-1)-sel)./((sel-1)*(1-gama_temp))))*((sel-(sel-1)*y)./(sel-(sel-1)*yf_temp))

      h=(y-yf_temp)./5
```

```
        y1=yf_temp+h
        y2=yf_temp+2*h
        y3=yf_temp+3*h
        y4=yf_temp+4*h

        f_y1=((y1./yf_temp).^((gama_temp*(sel-1)+1)./((sel-1)*(1-gama_temp))))*(((1-y1)./(1-
yf_temp)).^((gama_temp*(sel-1)-sel)./((sel-1)*(1-gama_temp))))*((sel-(sel-1)*y1)./(sel-(sel-
1)*yf_temp))
        f_y2=((y2./yf_temp).^((gama_temp*(sel-1)+1)./((sel-1)*(1-gama_temp))))*(((1-y2)./(1-
yf_temp)).^((gama_temp*(sel-1)-sel)./((sel-1)*(1-gama_temp))))*((sel-(sel-1)*y2)./(sel-(sel-
1)*yf_temp))
        f_y3=((y3./yf_temp).^((gama_temp*(sel-1)+1)./((sel-1)*(1-gama_temp))))*(((1-y3)./(1-
yf_temp)).^((gama_temp*(sel-1)-sel)./((sel-1)*(1-gama_temp))))*((sel-(sel-1)*y3)./(sel-(sel-
1)*yf_temp))
        f_y4=((y4./yf_temp).^((gama_temp*(sel-1)+1)./((sel-1)*(1-gama_temp))))*(((1-y4)./(1-
yf_temp)).^((gama_temp*(sel-1)-sel)./((sel-1)*(1-gama_temp))))*((sel-(sel-1)*y4)./(sel-(sel-
1)*yf_temp))

        f=(2*W*QO2_d*P./uf)-(1.0./(sel*(1-gama_temp)))*(sel-(sel-1)*yf_temp-(sel-(sel-
1)*y)*(((y./yf_temp).^((gama_temp*(sel-1)+1)./((sel-1)*(1-gama_temp))))*(((1-y)./(1-
yf_temp)).^((gama_temp*(sel-1)-sel)./((sel-1)*(1-gama_temp))))*((sel-(sel-1)*y)./(sel-(sel-
1)*yf_temp)))-(sel-1)*(h./2)*(f_yf_temp+2*f_y1+2*f_y2+2*f_y3+2*f_y4+f_yr_arb))
        endfunction

        yres(i)=fsolve(yr_arb,fex,1e-15)
        yres_temp=yres(i)

        Ur(i)=Uf*(((yres(i)/yf(i))^((gama(i)*(sel-1)+1)/((sel-1)*(1-gama(i)))))*(((1-yres(i))/(1-
yf(i)))^((gama(i)*(sel-1)-sel)/((sel-1)*(1-gama(i)))))*((sel-(sel-1)*yres(i))/(sel-(sel-1)*yf(i))))
        ur(i)=uf*(((yres(i)/yf(i))^((gama(i)*(sel-1)+1)/((sel-1)*(1-gama(i)))))*(((1-yres(i))/(1-
yf(i)))^((gama(i)*(sel-1)-sel)/((sel-1)*(1-gama(i)))))*((sel-(sel-1)*yres(i))/(sel-(sel-1)*yf(i))))

        function g=gex(x)
        g=(yres_temp/(1-yres_temp))-((sel*(x-gama_temp*(yres_temp)))/(1-x-gama_temp*(1-
yres_temp)))
        endfunction

        xres(i)=fsolve(xf,gex,1e-15)
    end

    for e=2:pts
        V(1)=0
        V(e)=uf*((L/(pts-1))*(e-1)-(L/(pts-1))*(e-2))-((((L/(pts-1))*(e-1)-(L/(pts-1))*(e-2))*(ur(e)+ur(e-
1)))/2)+V(e-1)
        Vy(1)=0
        Vy(e)=uf*xf*((L/(pts-1))*(e-1)-(L/(pts-1))*(e-2))-((((L/(pts-1))*(e-1)-(L/(pts-1))*(e-
2))*(xres(e)*ur(e)+xres(e-1)*ur(e-1)))/2)+Vy(e-1)

        Q(1)=0
        Q(e)=((V(e)*R*T)/(P*gama(e)))*60*10^3 // caudal permeado L/min
        Qp(e)=Q(e)*P*gama(e)*10^-5 // caudal a 1 bar

        y(1)=0
```

```
        y(e)=Vy(e)/V(e)

        y_m(1)=0
        y_m(e)=(y(e)*(3*16))/(y(e)*(3*16)+(1-y(e))*(2*16))
    end

    for a=1:pts-1
        p_2(pts)=P0^2
        parcela_1(pts-a)=(L/(pts-1)*((pts+1-a)-(pts-a)))/2
        parcela_2(pts-a)=(V(pts+1-a)*(visc_O3*y(pts+1-a)+visc_O2*(1-y(pts+1-a))))+(V(pts-
a)*(visc_O3*y(pts-a)+visc_O2*(1-y(pts-a))))

        p_2(pts-a)=p_2(pts+1-a)-(const*parcela_1(pts-a)*parcela_2(pts-a))

        p_nova(pts)=P0
        p_nova(pts-a)=sqrt(p_2(pts-a))

        gama_novo(pts)=P0/P
        gama_novo(pts-a)=sqrt(p_2(pts-a))/P
    end

    erro=abs(gama-gama_novo)
    soma=sum(erro)/12

    disp(1)
end

scf()
subplot(1,3,1)
plot(z,Qp(:))
xlabel('z / cm');ylabel('Caudal permeado total / L.min-1')
subplot(1,3,2)
plot(z,y_m(:))
xlabel('z / cm');ylabel('Fração mássica O3')
subplot(1,3,3)
plot(z,p_nova(:)*10^-5)
xlabel('z / cm');ylabel('Pressão permeado total / bar')
```

## A1.2 Hollow Fiber Membrane

### A1.2.1 Counter-current flow

```
clear
global Qswm Vswm Qf Qi Nf Dlm de di L tm sel LpO3 LpO2 yi0 Pti Pte R T pts
Nf = 80 // nº de fibras/capilares; L = 1 // m - comprimento
di = 2*0.0005 // m - diâmatro interno; tm = 0.0005 // m - espessura da membrana
de = di+(2*tm) // m - diâmetro externo
Dlm = Nf*((%pi*de)-(%pi*di))/log(de/di)

sel = 4
LpO2 = 2.81*10^-13; LpO3 = sel*LpO2 // mol/(m s Pa)

R = 8.314 // m3 Pa K-1 mol-1; T = 273.15+25 // K
```

```
Pti = 6*10^5 // Pa alimentação; Pte = 1*10^5 // Pa permeado

Qi = ((1*10^-3)/60)/(Pti*10^-5) // m3/s - caudal interior a Pti
yi0 = (0.13/(3*16))/(0.13/(3*16)+0.87/(2*16)) // fração molar O3 à entrada no interior da fibra

pts=30

function f=fex(x, y)
    f(1)=-Dlm*(LpO3/tm)*(Pti*(y(1)/(y(1)+y(2)))-Pte*(y(3)/(y(3)+y(4))))
    f(2)=-Dlm*(LpO2/tm)*(Pti*(y(2)/(y(1)+y(2)))-Pte*(y(4)/(y(3)+y(4))))
    f(3)=-Dlm*(LpO3/tm)*(Pti*(y(1)/(y(1)+y(2)))-Pte*(y(3)/(y(3)+y(4))))
    f(4)=-Dlm*(LpO2/tm)*(Pti*(y(2)/(y(1)+y(2)))-Pte*(y(4)/(y(3)+y(4))))
endfunction

x0=0;xf=L;y0=[(Qi*yi0*Pti)/(R*T);(Qi*(1-yi0)*Pti)/(R*T);2.3641*10^-5;9.6*10^-5]
x=x0:(L/(pts-1)):xf
z=x'
y=ode(y0,x0,x,fex)
F=y'

for i=1:pts
    yO3_int(i)=F(i,1)/(F(i,1)+F(i,2))
    yO2_int(i)=F(i,2)/(F(i,1)+F(i,2))
    pO3_int(i)=yO3_int(i)*Pti*10^-5
    pO2_int(i)=yO2_int(i)*Pti*10^-5

    Qint_O3(i)=((F(i,1)*R*T)/Pti)*60*10^3 // caudal permeado L/min
    Q_O3(i)=Qint_O3(i)*Pti*10^-5 // caudal a 1 bar
    Qint_O2(i)=((F(i,2)*R*T)/Pti)*60*10^3 // caudal permeado L/min
    Q_O2(i)=Qint_O2(i)*Pti*10^-5 // caudal a 1 bar

    Qext_O3(i)=((F(i,3)*R*T)/Pte)*60*10^3 // caudal permeado L/min
    Qp_O3(i)=Qext_O3(i)*Pte*10^-5 // caudal a 1 bar
    Qext_O2(i)=((F(i,4)*R*T)/Pte)*60*10^3 // caudal permeado L/min
    Qp_O2(i)=Qext_O2(i)*Pte*10^-5 // caudal a 1 bar

    V(i)=F(i,3)+F(i,4)
    Qp_total(i)=(F(i,3)+F(i,4))*R*T*60*10^3*10^-5 // caudal total permeado L/min
end

pO3_ext(pts)=0; pO2_ext(pts)=0; yO3_ext(pts)=0; yO2_ext(pts)=0
yO3_m(pts)=0

for i=1:pts-1
    yO3_ext(i)=F(i,3)/(F(i,3)+F(i,4))
    yO2_ext(i)=F(i,4)/(F(i,3)+F(i,4))
    pO3_ext(i)=yO3_ext(i)*Pte*10^-5
    pO2_ext(i)=yO2_ext(i)*Pte*10^-5

    yO3_m(i)=(yO3_ext(i)*3*16)/((yO3_ext(i)*3*16)+(yO2_ext(i)*2*16))
end

scf()
```

```
subplot(1,6,1)
plot(z,Q_O3(:),z,Qp_O3(:))
legend('interior','exterior',"upper_caption")
xlabel('z / m');ylabel('Q.O3 / L.min-1')
subplot(1,6,2)
plot(z,Q_O2(:),z,Qp_O2(:))
legend('interior','exterior',"upper_caption")
xlabel('z / m');ylabel('Q.O2 / L.min-1')
subplot(1,6,3)
plot(z,pO3_int(:),z,pO3_ext(:))
legend('interior','exterior',"upper_caption")
xlabel('z / m');ylabel('pO3 / bar')
subplot(1,6,4)
plot(z,pO2_int(:),z,pO2_ext(:))
legend('interior','exterior',"upper_caption")
xlabel('z / m');ylabel('pO2 / bar')
subplot(1,6,5)
plot(z,yO3_int(:),z,yO3_ext(:))
legend('interior','exterior',"upper_caption")
xlabel('z / m');ylabel('yO3 molar / bar')
subplot(1,6,6)
plot(z,yO2_int(:),z,yO2_ext(:))
legend('interior','exterior',"upper_caption")
xlabel('z / m');ylabel('yO2 molar / bar')
```

### A1.2.2 Co-current flow

```
clear
global Qswm Vswm Qf Qi Nf Dlm de di L tm sel LpO3 LpO2 yi0 Pti Pte R T pts
Nf = 80 // nº de fibras/capilares; L = 1 // m - comprimento
di = 2*0.0005 // m - diâmatro interno; tm = 0.0005 // m - espessura da membrana
de = di+(2*tm) // m - diâmetro externo
Dlm = Nf*((%pi*de)-(%pi*di))/log(de/di)

sel = 4
LpO2 = 2.81*10^-13; LpO3 = sel*LpO2 // mol/(m s Pa)

R = 8.314 // m3 Pa K-1 mol-1; T = 273.15+25 // K
Pti = 6*10^5 // Pa alimentação; Pte = 1*10^5 // Pa permeado

Qi = ((1*10^-3)/60)/(Pti*10^-5) // m3/s - caudal interior a Pti
yi0 = (0.13/(3*16))/(0.13/(3*16)+0.87/(2*16)) // fração molar O3 à entrada no interior da fibra

pts=30

function f=fex(x, y)
   f(1)=-Dlm*(LpO3/tm)*(Pti*(y(1)/(y(1)+y(2)))-Pte*(y(3)/(y(3)+y(4))))
   f(2)=-Dlm*(LpO2/tm)*(Pti*(y(2)/(y(1)+y(2)))-Pte*(y(4)/(y(3)+y(4))))
   f(3)=Dlm*(LpO3/tm)*(Pti*(y(1)/(y(1)+y(2)))-Pte*(y(3)/(y(3)+y(4))))
   f(4)=Dlm*(LpO2/tm)*(Pti*(y(2)/(y(1)+y(2)))-Pte*(y(4)/(y(3)+y(4))))
endfunction
```

```
x0=0;xf=L;y0=[(Qi*yi0*Pti)/(R*T);(Qi*(1-yi0)*Pti)/(R*T);1e-10;1e-10]
x=x0:(L/(pts-1)):xf
z=x'
y=ode(y0,x0,x,fex)
F=y'

for i=1:pts
   yO3_int(i)=F(i,1)/(F(i,1)+F(i,2))
   yO2_int(i)=F(i,2)/(F(i,1)+F(i,2))
   pO3_int(i)=yO3_int(i)*Pti*10^-5
   pO2_int(i)=yO2_int(i)*Pti*10^-5

   Qint_O3(i)=((F(i,1)*R*T)/Pti)*60*10^3 // caudal permeado L/min
   Q_O3(i)=Qint_O3(i)*Pti*10^-5 // caudal a 1 bar
   Qint_O2(i)=((F(i,2)*R*T)/Pti)*60*10^3 // caudal permeado L/min
   Q_O2(i)=Qint_O2(i)*Pti*10^-5 // caudal a 1 bar
end

pO3_ext(1)=0; pO2_ext(1)=0; yO3_ext(1)=0; yO2_ext(1)=0
Qext_O3(1)=0;Qext_O2(1)=0;Qp_O3(1)=0;Qp_O2(1)=0;Qp_total(1)=0; V(1)=0
yO3_m(1)=0

for i=2:pts
   yO3_ext(i)=F(i,3)/(F(i,3)+F(i,4))
   yO2_ext(i)=F(i,4)/(F(i,3)+F(i,4))
   pO3_ext(i)=yO3_ext(i)*Pte*10^-5
   pO2_ext(i)=yO2_ext(i)*Pte*10^-5

   yO3_m(i)=(yO3_ext(i)*3*16)/((yO3_ext(i)*3*16)+(yO2_ext(i)*2*16))

   Qext_O3(i)=((F(i,3)*R*T)/Pte)*60*10^3 // caudal permeado L/min
   Qp_O3(i)=Qext_O3(i)*Pte*10^-5 // caudal a 1 bar
   Qext_O2(i)=((F(i,4)*R*T)/Pte)*60*10^3 // caudal permeado L/min
   Qp_O2(i)=Qext_O2(i)*Pte*10^-5 // caudal a 1 bar

   V(i)=F(i,3)+F(i,4)
   Qp_total(i)=(F(i,3)+F(i,4))*R*T*60*10^3*10^-5 // caudal total permeado L/min
end

scf()
subplot(1,6,1)
plot(z,Q_O3(:),z,Qp_O3(:))
legend('interior','exterior',"upper_caption")
xlabel('z / m');ylabel('Q.O3 / L.min-1')
subplot(1,6,2)
plot(z,Q_O2(:),z,Qp_O2(:))
legend('interior','exterior',"upper_caption")
xlabel('z / m');ylabel('Q.O2 / L.min-1')
subplot(1,6,3)
plot(z,pO3_int(:),z,pO3_ext(:))
legend('interior','exterior',"upper_caption")
xlabel('z / m');ylabel('pO3 / bar')
subplot(1,6,4)
```

```
plot(z,pO2_int(:),z,pO2_ext(:))
legend('interior','exterior',"upper_caption")
xlabel('z / m');ylabel('pO2 / bar')
subplot(1,6,5)
plot(z,yO3_int(:),z,yO3_ext(:))
legend('interior','exterior',"upper_caption")
xlabel('z / m');ylabel('yO3 molar / bar')
subplot(1,6,6)
plot(z,yO2_int(:),z,yO2_ext(:))
legend('interior','exterior',"upper_caption")
xlabel('z / m');ylabel('yO2 molar / bar')
```

### A1.2.3 Cross-flow

```
clear
global Qswm Vswm Qf Qi Nf Dlm de di L tm sel LpO3 LpO2 yi0 Pti Pte gama R T pts
Nf = 80 // nº de fibras/capilares; L = 1 // m - comprimento
di = 2*0.0005 // m - diâmatro interno; tm = 0.0005 // m - espessura da membrana
de = di+(2*tm) // m - diâmetro externo
Dlm = Nf*((%pi*de)-(%pi*di))/log(de/di)

sel = 4
LpO2 = 2.81*10^-13; LpO3 = sel*LpO2 // mol/(m s Pa)
R = 8.314 // m3 Pa K-1 mol-1; T = 273.15+25 // K
Pti = 6*10^5 // Pa alimentação; Pte = 1*10^5 // Pa permeado
gama = Pte/Pti
Qi = ((1*10^-3)/60)/(Pti*10^-5) // m3/s - caudal interior a Pti
yi0 = (0.13/(3*16))/(0.13/(3*16)+0.87/(2*16)) // fração molar O3 à entrada no interior da fibra
pts=30

function f=fex(x, y)
   f(1)=-Dlm*(LpO3/tm)*(Pti*(y(1)/(y(1)+y(2)))-Pte*((1+(sel-1)*(gama+(y(1)/(y(1)+y(2))))-sqrt((1+(sel-
1)*(gama+(y(1)/(y(1)+y(2)))))^2-4*gama*sel*(sel-1)*(y(1)/(y(1)+y(2)))))/(2*gama*(sel-1))))
   f(2)=-Dlm*(LpO2/tm)*(Pti*(y(2)/(y(1)+y(2)))-Pte*((1+(sel-1)*(gama+(y(2)/(y(1)+y(2))))-sqrt((1+(sel-
1)*(gama+(y(2)/(y(1)+y(2)))))^2-4*gama*sel*(sel-1)*(y(2)/(y(1)+y(2)))))/(2*gama*(sel-1))))
   f(3)=Dlm*(LpO3/tm)*(Pti*(y(1)/(y(1)+y(2)))-Pte*((1+(sel-1)*(gama+(y(1)/(y(1)+y(2))))-sqrt((1+(sel-
1)*(gama+(y(1)/(y(1)+y(2)))))^2-4*gama*sel*(sel-1)*(y(1)/(y(1)+y(2)))))/(2*gama*(sel-1))))
   f(4)=Dlm*(LpO2/tm)*(Pti*(y(2)/(y(1)+y(2)))-Pte*((1+(sel-1)*(gama+(y(2)/(y(1)+y(2))))-sqrt((1+(sel-
1)*(gama+(y(2)/(y(1)+y(2)))))^2-4*gama*sel*(sel-1)*(y(2)/(y(1)+y(2)))))/(2*gama*(sel-1))))
endfunction

x0=0;xf=L;y0=[(Qi*yi0*Pti)/(R*T);(Qi*(1-yi0)*Pti)/(R*T);1e-10;1e-10]
x=x0:(L/(pts-1)):xf
z=x'
y=ode(y0,x0,x,fex)
F=y'

for i=1:pts
   yO3_int(i)=F(i,1)/(F(i,1)+F(i,2))
   yO2_int(i)=F(i,2)/(F(i,1)+F(i,2))
   pO3_int(i)=yO3_int(i)*Pti*10^-5
   pO2_int(i)=yO2_int(i)*Pti*10^-5
```

```
    Qint_O3(i)=((F(i,1)*R*T)/Pti)*60*10^3 // caudal permeado L/min
    Q_O3(i)=Qint_O3(i)*Pti*10^-5 // caudal a 1 bar
    Qint_O2(i)=((F(i,2)*R*T)/Pti)*60*10^3 // caudal permeado L/min
    Q_O2(i)=Qint_O2(i)*Pti*10^-5 // caudal a 1 bar
end

pO3_ext(1)=0; pO2_ext(1)=0; yO3_ext(1)=0; yO2_ext(1)=0
Qext_O3(1)=0;Qext_O2(1)=0;Qp_O3(1)=0;Qp_O2(1)=0;Qp_total(1)=0
yO3_m(1)=0

for i=2:pts
    yO3_ext(i)=F(i,3)/(F(i,3)+F(i,4))
    yO2_ext(i)=F(i,4)/(F(i,3)+F(i,4))
    pO3_ext(i)=yO3_ext(i)*Pte*10^-5
    pO2_ext(i)=yO2_ext(i)*Pte*10^-5

    yO3_m(i)=(yO3_ext(i)*3*16)/((yO3_ext(i)*3*16)+(yO2_ext(i)*2*16))

    Qext_O3(i)=((F(i,3)*R*T)/Pte)*60*10^3 // caudal permeado L/min
    Qp_O3(i)=Qext_O3(i)*Pte*10^-5 // caudal a 1 bar
    Qext_O2(i)=((F(i,4)*R*T)/Pte)*60*10^3 // caudal permeado L/min
    Qp_O2(i)=Qext_O2(i)*Pte*10^-5 // caudal a 1 bar

    V(i)=F(i,3)+F(i,4)
    Qp_total(i)=(F(i,3)+F(i,4))*R*T*60*10^3*10^-5 // caudal total permeado L/min
end

scf()
subplot(1,6,1)
plot(z,Q_O3(:),z,Qp_O3(:))
legend('interior','exterior',"upper_caption")
xlabel('z / m');ylabel('Q.O3 / L.min-1')
subplot(1,6,2)
plot(z,Q_O2(:),z,Qp_O2(:))
legend('interior','exterior',"upper_caption")
xlabel('z / m');ylabel('Q.O2 / L.min-1')
subplot(1,6,3)
plot(z,pO3_int(:),z,pO3_ext(:))
legend('interior','exterior',"upper_caption")
xlabel('z / m');ylabel('pO3 / bar')
subplot(1,6,4)
plot(z,pO2_int(:),z,pO2_ext(:))
legend('interior','exterior',"upper_caption")
xlabel('z / m');ylabel('pO2 / bar')
subplot(1,6,5)
plot(z,yO3_int(:),z,yO3_ext(:))
legend('interior','exterior',"upper_caption")
xlabel('z / m');ylabel('yO3 molar / bar')
subplot(1,6,6)
plot(z,yO2_int(:),z,yO2_ext(:))
legend('interior','exterior',"upper_caption")
xlabel('z / m');ylabel('yO2 molar / bar')
```

# Appendix 2 Simulation results (graphs)

## A2.1 Hollow Fiber Membrane

### A2.1.1 Co-current flow

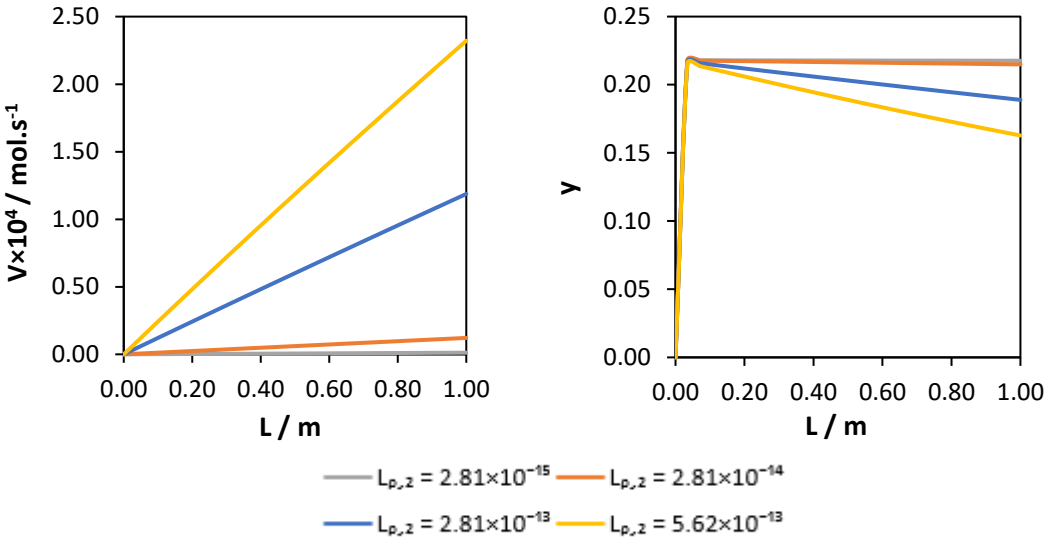


*Figure 28 – Simulation outputs along the membrane length, with membrane permeability of $O_2$ variation*

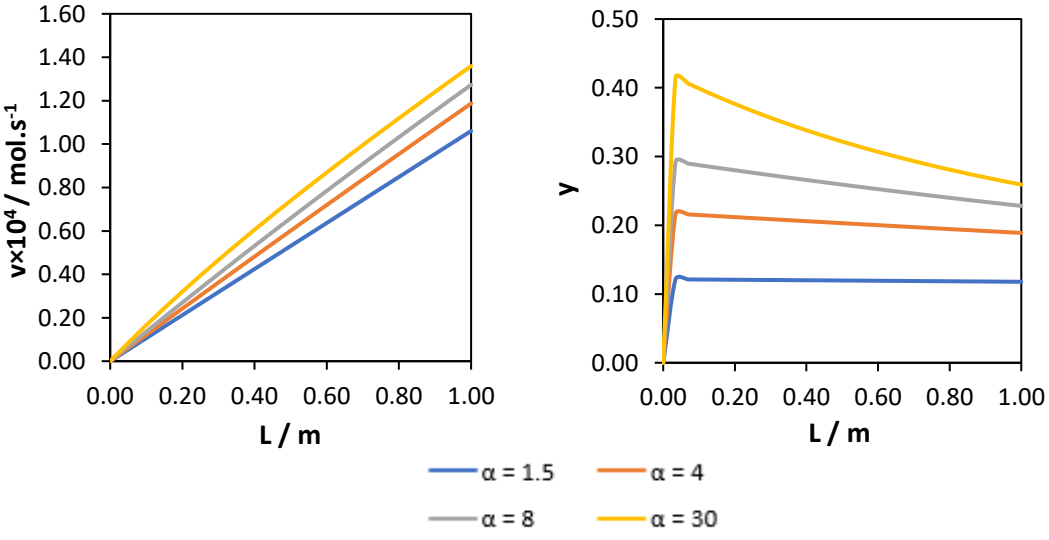


*Figure 29 – Simulation outputs along the membrane length, with selectivity variation*

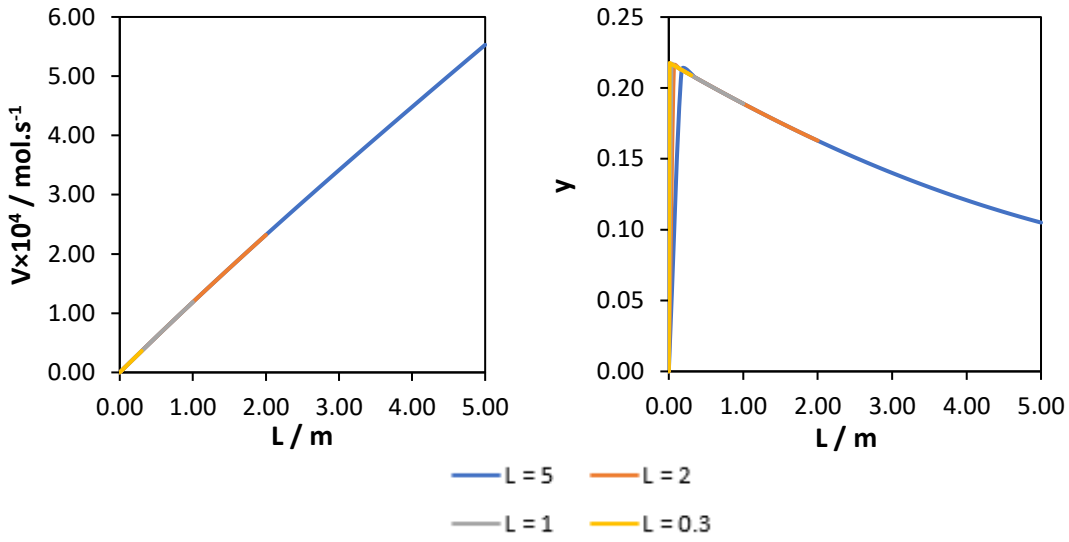


*Figure 30 - Simulation outputs along the membrane length, with length variation*

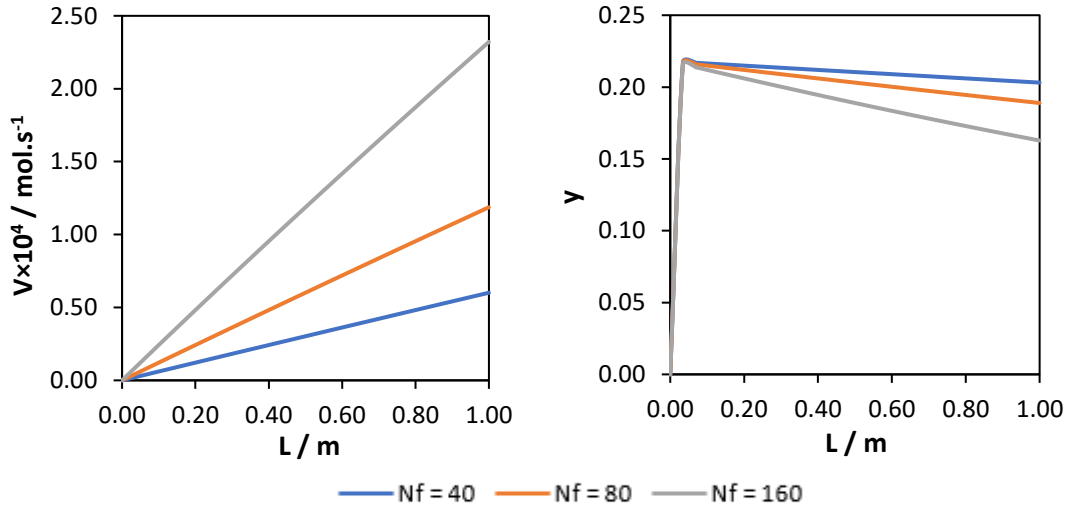


*Figure 31 - Simulation outputs along the membrane length, with number of fibers variation*

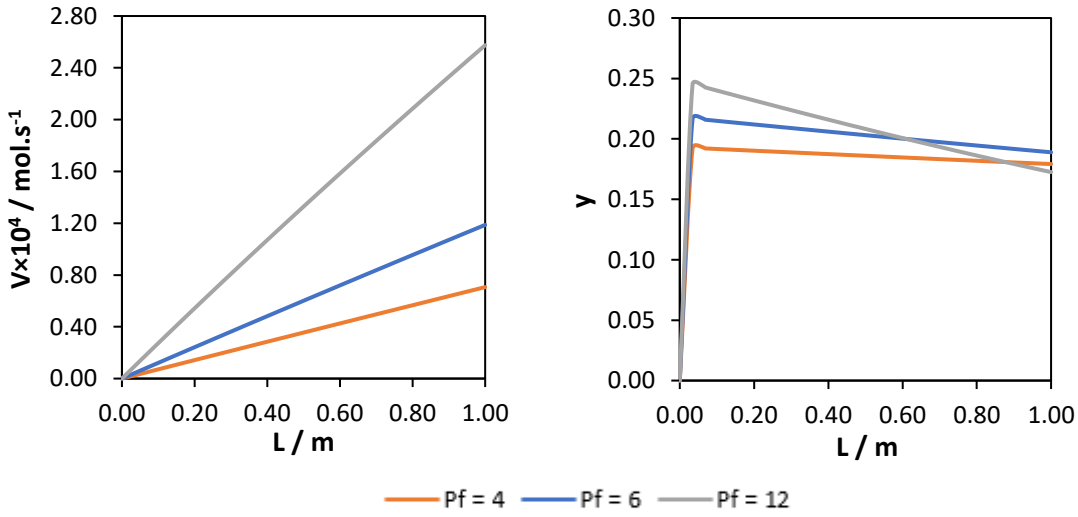


*Figure 32 - Simulation outputs along the membrane length, with feed pressure variation*

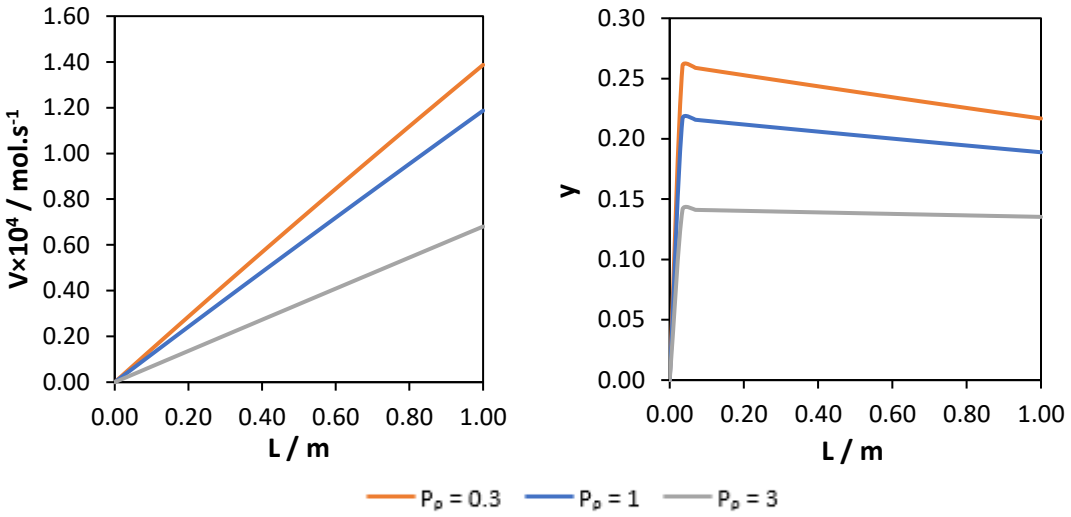


*Figure 33 – Simulation outputs along the membrane length, with permeate pressure variation*

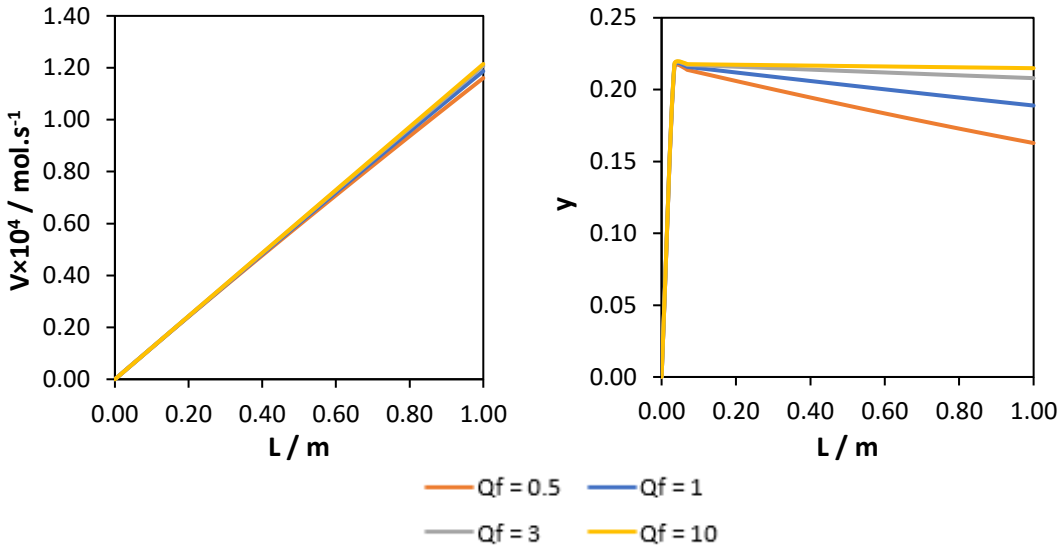


*Figure 34 – Simulation outputs along the membrane length, with feed flow rate variation*

### A2.1.2 Cross-flow

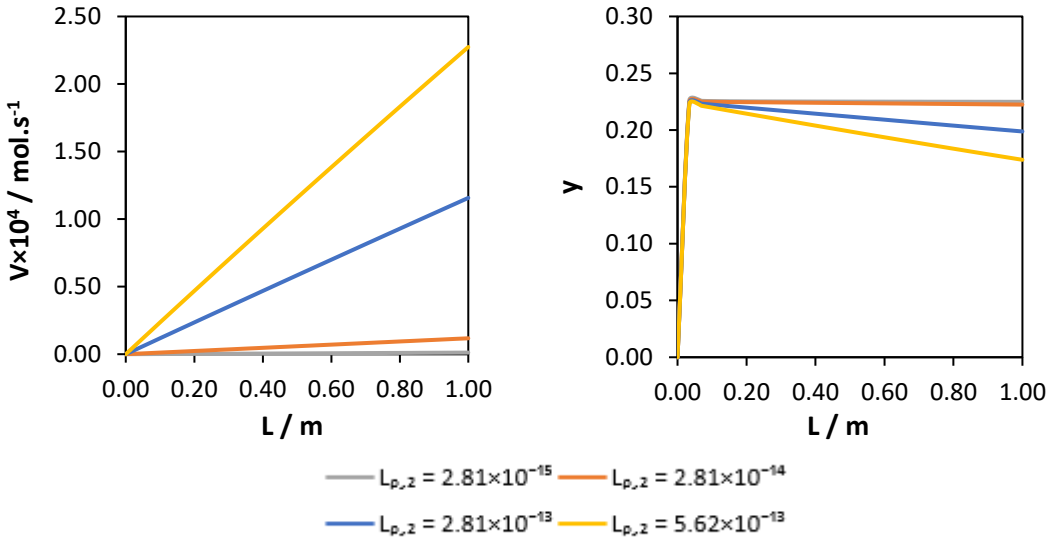


*Figure 35 – Simulation outputs along the membrane length, with membrane permeability of $O_2$ variation*

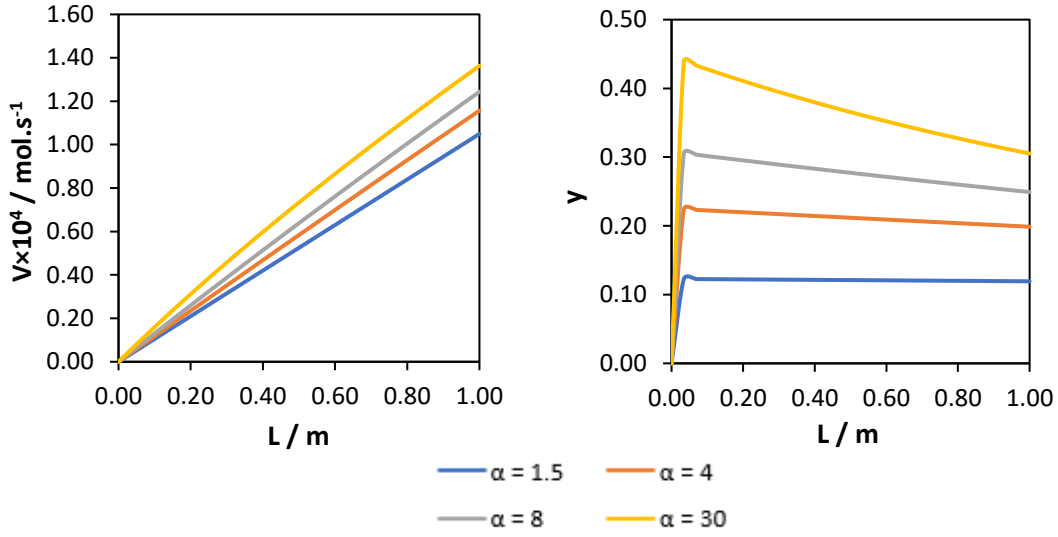


*Figure 36 – Simulation outputs along the membrane length, with selectivity variation*

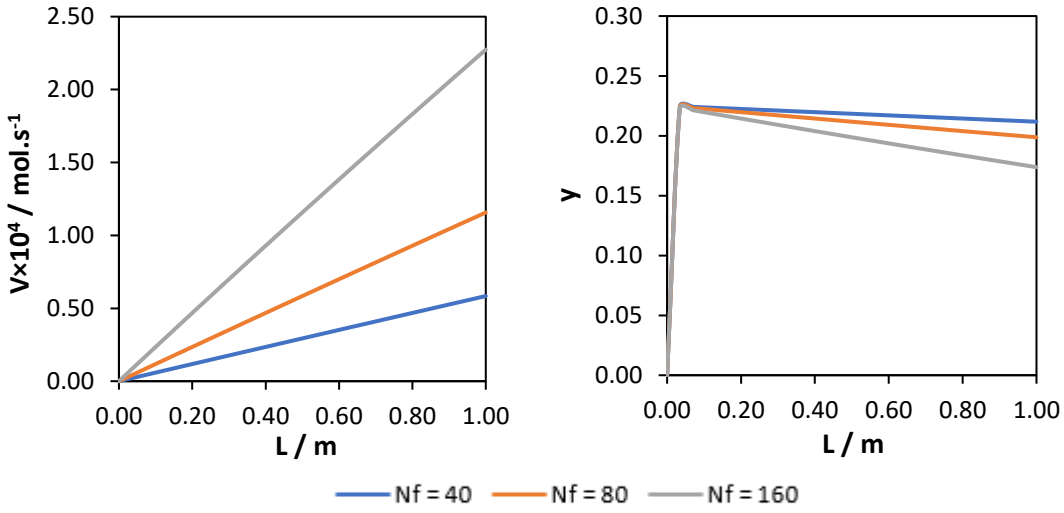


*Figure 37 - Simulation outputs along the membrane length, with number of fibers variation*

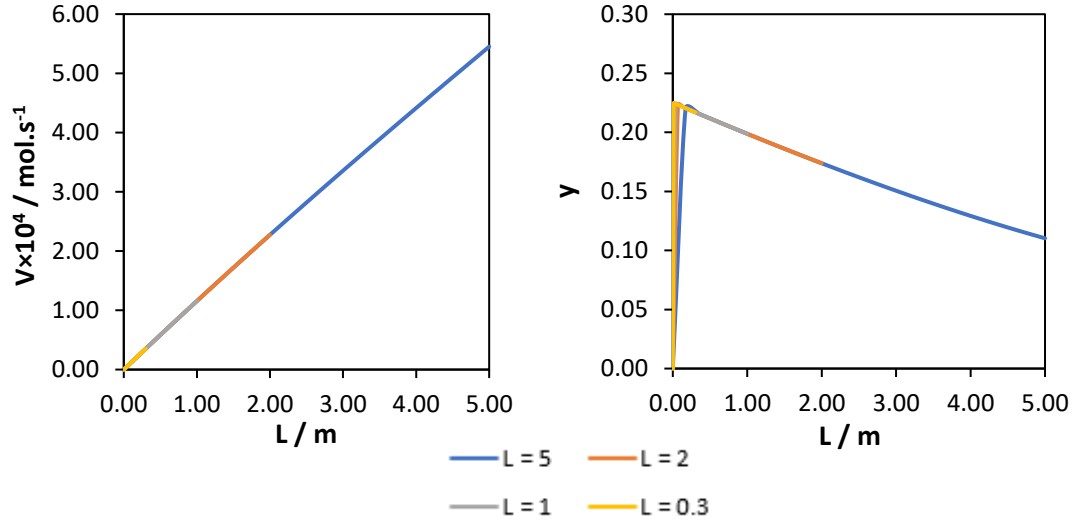


*Figure 38 - Simulation outputs along the membrane length, with length variation*

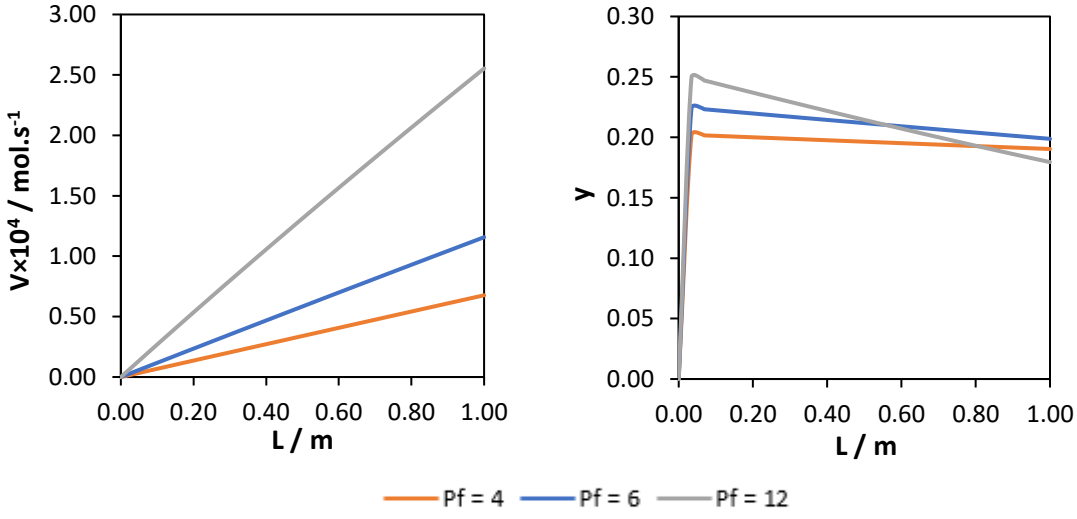


*Figure 39 - Simulation outputs along the membrane length, with feed pressure variation*

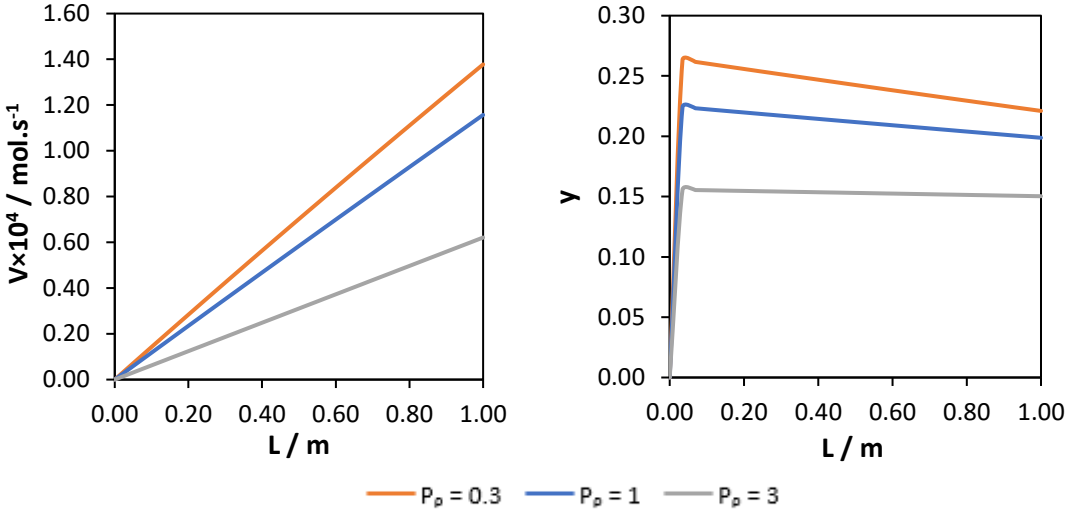


*Figure 40 - Simulation outputs along the membrane length, with permeate pressure variation*

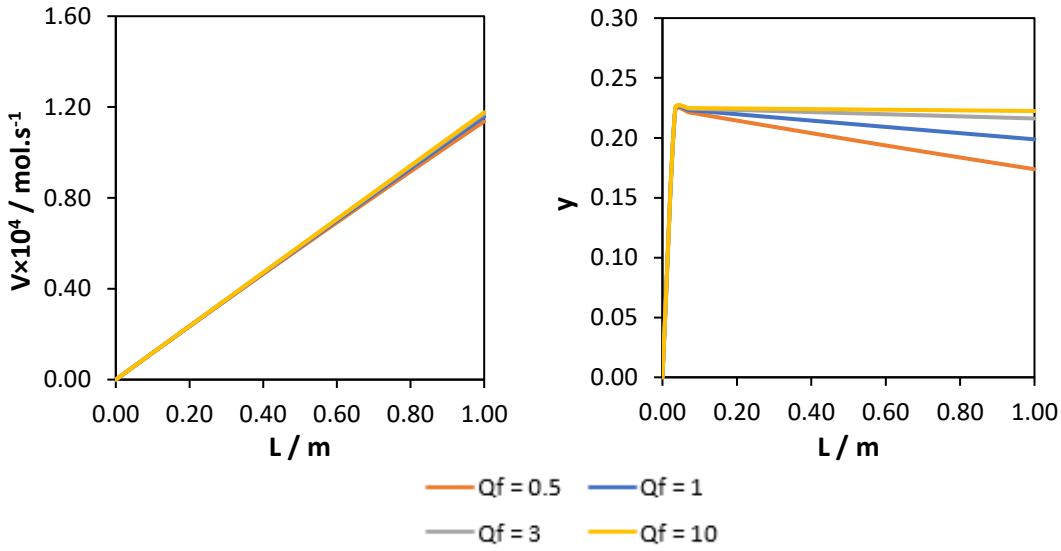


*Figure 41 - Simulation outputs along the membrane length, with feed flow rate variation*

# Appendix 3 Calculation procedure for the experimental data

In the experimental tests, it was controlled the feed flow rate and measured the retentate flow rate and the ozone concentration in the feed and the retentate streams. The values obtained are in Table 10.

*Table 10 – Experimental data measured*

| **Feed** | | **Retentate** | |
|---|---|---|---|
| $Q_f$ (STP L·min$^{-1}$) | $C_{O_3}$ (g·Nm$^{-3}$) | $Q_r$ (L·min$^{-1}$) | $C_{O_3}$ (g·Nm$^{-3}$) |
| 0.6 | 83.3 | 0.47 | 77.9 |
| 0.5 | 100.0 | 0.38 | 91.5 |
| 0.4 | 125.8 | 0.28 | 111.4 |
| 0.3 | 161.9 | 0.20 | 131.6 |
| 0.5 | 100.2 | 0.37 | 93.6 |
| 0.4 | 100.0 | 0.28 | 90.6 |
| 0.3 | 100.5 | 0.20 | 89.4 |

Feed flow rate was in standard conditions (0 °C and 1 bar) and ozone concentration was measured in normal conditions (20 °C and 1 bar), so first these values were converted to environmental conditions (25 °C and 1 bar), using the ideal gas law (Equation 22).

$$nRT = Pv \tag{22}$$

Then, by multiplying the total flow rate with the ozone concentration and converting grams to moles and minutes to seconds, it was obtained the ozone flow rate, in mol·s$^{-1}$. The total flow rate, in mol·s$^{-1}$, was determined using again Equation 22.

As for the ozone molar fraction, it was calculated through the ozone concentration of Table 10, in environment conditions, the ozone molecular weight and the ideal gas law.

The permeate flow rate and composition was determined by basically subtracting the retentate flow rate to the feed flow rate.